Simulation of Fatigue Performance & Creep Rupture of Glass-Reinforced Polymeric Composites for Infrastructure Applications

By

David Fred M^{c}Bagonluri-Nuuri

Thesis submitted to the Faculty of the
Virginia Polytechnic Institute and State University
in partial fulfillment of the requirements for the degree of

Master of Science
in
Engineering Mechanics

John J. Lesko, Chair
Scott Case
David Gao
David Dillard

August 18, 1998
Blacksburg, Virginia

Keywords: Glass Composites, Fatigue, Environmental Effects, Lattice Green's Function, Creep Rupture, Fiber Bundle, Local Load Sharing

Simulation of Fatigue Performance & Creep Rupture of Glass-Reinforced Polymeric Composites for Infrastructure Applications

DAVID FRED M^{C}BAGONLURI-NUURI

John J. Lesko, Chair

Engineering Science & Mechanics

(ABSTRACT)

A simulation model which incorporates the statistical- and numerical-based Lattice Green Function Local Load Sharing Model and a Fracture Mechanics-based Residual Strength Model has been developed. The model simulates creep rupture by imposing a fixed load of constant stress on the composite over the simulation duration. Simulation of the fatigue of glass fiber-reinforced composites is achieved by replacing the constant stress parameter in the model with a sinusoidal wave function. Results from the creep rupture model using fused silica fiber parameters, compare well with S-2 glass/epoxy systems. Results using Mandell's postulate that fatigue failure in glass fiber-reinforced polymeric composites is a fiber-dominated mechanism, with a characteristic slope of 10 %UTS/decade are consistent with available experimental data. The slopes of fatigue curves for simulated composites for three frequencies namely: 2, 5 and 10 Hz are within 12-14 %UTS/decade compared with that of 10.6-13.0 %UTS/decade for unidirectional glass reinforced composites (epoxy and vinyl ester) obtained from Demers' [40] data.

ACKNOWLEDGMENTS

I wish to acknowledge the following individuals whose enormous contributions led to the successful completion of this thesis:

- **Dr. John Lesko**, thanks for your immense contribution to my academic advancement and your tremendous patience during many challenging moments. A man of limitless patience, “if I have come and seen far it is because I stood on your shoulders.” Your future is limitless. I am glad to have been associated with you. When I become President of Ghana you get the red carpet!

- **Dr. David Gao**, thanks for his ennobling association. Thanks for giving me another dimension to life.
- **Dr. David Dillard,** thanks for taking time off your busy schedule to serve on my committee.

- **Dr. Scott Case**, thanks for the tremendous help you offered for the simulation section of this thesis. Your guidance and assistance were priceless.

- Thanks to **Bev Williams, Sheila Collins, and Loretta Tickle** without whom the MRG and ESM will come crumbling like the Berlin Wall!

- **Dr. Moussa Wone**, thanks for all your assistance in the development of my codes and for introducing me to the UNIX system. You are a true great friend and one of the finest minds I have ever known. Your association has privileged me.

- **Dr. Kenneth Reifsnider**, thanks for the opportunity to take your course on the Mechanics of Composites Life & Strength and for your concern and care for your students.

- **Dr. Byung-Kim Ahn,** a man of tremendous spiritual power and unparalleled humility, and who I have been privilege to know for many years.

- **Mr. Mike Pastor,** an American patriot, I'll remember you for your unflinching positions during our after-lunch debates, and for your remarkable insight on world affairs.

- **Jean M. Bodin,** for your friendship and ennobling association.

- **Dr. and Mrs. Kala Seidu,** thanks for your support and vision and for your ennobling association. I am privileged to call you my own.

- **Mr. Mac McCord,** thanks for the design phase of my project. Mac has insight on even the most unthinkable. A real life jack-of-all-trades and master of all!

- **Xinyu Huang,** thanks for the many questions on UNIX that you were ever-present to answer. I am will miss your friendship.

- **Celine Mahieux**, thanks for your friendship and concern. You made the work a little easier with your caring words and advice.

- **Dr. Judy Wood**, thanks teaching me how to coat my specimens and how to use the *INSTRON* and your friendship. Thanks!

- **Dr. Joanine Chin**, NIST, for your interest in my research and for your support. Your future as a scientist is limitless!

- **Ben Tatuo, Francis Martin, Derrick Dlamini, Sam Suraphel, Juone Brown, Newland Agbenowosi,** you have been my pillar and my strength through many trying times. I am forever grateful for your love and for your kindness. The world will be a whole lot better with your kind.

- **Hala Ahmed,** thanks for your friendship.

- **Lutfah Issah**, you are that very special person in my life, and that is why it so complete!

- **Mahtsente Worku,** you will always be my mirror to life. I am thankful for your great friendship and love through many challenging times. I am very fortunate to have known you. You gave me a new insight into what courage and perseverance really meant. You are always my heroine and my baby!

- **Kingsley,** you are the best uncle in the world. I am thankful for your love and your support. You are my pillar and my strength, my fountain of knowledge. Your courage and steadfastness have been a source of inspiration for many generations of Bagonluris. You are our pride and pearl!

- **Hon. Alhaji Mahama Iddrisu,** thanks for being the best uncle that you are and for serving the People of Ghana for nearly two decades as Secretary of Defense. You are a Statesman's Statesman!

- **Regina W. Bagonluri,** you're the best aunt, the very best! You were my

greatest support through many trying moments and a continuous source of inspiration.

- **Saeed Zakaria Foroko,** University of Cape Coast, Ghana. Thanks for your many years of great friendship. What a tremendous human being? You never cease to baffle me with your integrity, patience and perseverance.
- **Dr. and Mrs. Telih Boyiri,** your are my true great cousins, and so are you Telih Jr. and Thelma.

Finally, I'll like to thank my mother, Patience for your strength and patience. You were a lioness that protected her your own with such ferocity*. If it takes a village, it certainly takes a mother too!* My siblings, the Rev. Thomas, Gad, Maxwell and Linda, my aunts Martha, Agnes, Cecilia, my cousins Anita, Noor, Baba, Pauline and the Bagonluri Clan of Wa, Ollo and Korinyiri, your are all very special and dear to me.

DEDICATION

This thesis is dedicated to the memory of my late maternal grandparents and my late father:

BOYE NINSIA NUURI

POGPILLA KOMA NUURI

HON. DAVID ANG-LAARA MACBAGONLURI

And to

MY COUSIN, NOOR FOR YOUR 2ND BIRTHDAY

MY AUNT, REGINA WURUCHE BAGONLURI

MY MOM, PATIENCE ASIBI NUURI

HON. ALHAJI MAHAMA IDDRISU,

MINISTER OF DEFENSE, REPUBLIC OF GHANA

TABLE OF CONTENTS

LIST OF FIGURES

LIST OF TABLES

Chapter 1 : INTRODUCTION AND OBJECTIVES

1.1 Introduction: Recent Advances in Composite Application

There has been, in recent times, a significant rise in the application of composite materials in industry. This surging interest in composite materials over traditional engineering materials has been the result of increasing knowledge and research on the properties of composite materials (i.e. tailorability, corrosion advantages, and high strength-to-weight ratio). The marine, civil, and petrochemical industries are all harnessing the advantages of advanced composite materials for numerous applications.

In the marine sector, composites are finding application in ship, submarine and hovercraft construction. Recent application of composites in the marine arena has been undertaken by ADI Limited, an Australian Company contracted to build Six Huon Class mine-hunters for the Royal Australian Navy [1]. The British Royal Navy mine-hunter program was designed to provide parts for hovercrafts and submarines [2]. In the US, the MARITECH project, a joint industry and government venture was initiated to encourage the development of composite superstructure systems for commercial vessels [3]. Karlskronavarvet, a Swedish company, has developed a highspeed composite *Stealth vessel YS 2000 (Corvette type Visby)* as part of NATO's fleet for use in the North Atlantic [4].

The oil industry is harnessing composites for marine-based construction. This trend towards composite application in the offshore arena is due to the desire to reduce life-cycle cost in deepwater construction and the need for improved reliability. Another advantage composites offer is the innovative approach where fiber optics are embedded in the structure for purposes of remote monitoring of structural integrity [5]. Northrop Grumman Marine Systems is currently leading a joint venture to market lightweight composite tubulars for gas as well as deepwater oil exploration. The Institut Français du Pétrole and Aérospatiale has developed a composite production riser for reducing the required pretension and for simplifying the riser tension in oil exploration. Wellstream, Inc., has constructed an Intelligent Flexible Composite Pipe with an embedded performance monitor for use in gas and oil production [5].

FRP tanks and storage systems have found significant use in the petrochemical industry due to their internal and external corrosion resistance. Corrosion resistant storage systems have reduced considerably the risk of environmental related hazards such as spillage and percolation of toxins into the water table. The attractiveness of FRP storage facilities has been on the increase due to the potentially hazardous consequences steel tanks have posed lately. It has been noted by Norwood et al. [6] that out of the two million federally regulated storage units in the U.S., over 450,000 of these tanks are known to be leaking. This imminent threat to the environment is not confined to the U.S. As a matter of fact the situation parallels that of Great Britain where rapid increase in vehicle ownership led to increase in underground storage facilities for petroleum related products. Having outlived their useful design lives, these

facilities are deteriorating at an alarming rate and the threat they pose to the environment may have serious repercussions [6].

Composite bridges are springing up in their numbers, as advanced composites materials become available and less expensive. These bridges may be pedestrian bridges, such as LaSalle Street pedestrian walkway in Kentucky, or traffic bridges, such as the Tom's Creek Bridge at Blacksburg, VA constructed by the Materials Response Group at Virginia Tech. Other recent constructions containing composites are the Laurel Lick Bridge in Lewis County, West Virginia, and the Bonds Mill Lift Bridge in Stroud, England [7].

1.2 Introduction: Motivation

Insufficient knowledge of composite durability and the lack of life prediction methodologies for predicting glass fiber-reinforced composite material durability and damage tolerance are the mitigating factors against the readily acceptance of fiber-reinforced plastics (FRP) in the marine and civil infrastructure. In order to increase the use of composite materials in the infrastructure arena, the nature and effect of the service environment on the durability of glass fiber-reinforced composite materials must be investigated and appropriate methods established for assessing service life. The knowledge of the mechanics and kinetics of glass-polymer system degradation is essential for the formulation of analytical tools for the characterization of fiber-reinforced composites. The absence of a unified theory for the complete

characterization of glass fiber-reinforced composites systems is the major challenge facing the composite industry.

In addition to lack of predictive tools, the composite industry is also confronted with little data. The data currently available is industry-specific. Most of the data belong to the aerospace and petrochemical industries where years of exposure to composites have resulted in a databank while little data is currently available for the marine and infrastructure sectors. The absence of glass fiber-reinforced data for marine and infrastructure application where longevity is the objective function has been responsible for the slow acceptance of the use composites in the marine and infrastructure arena.

This growing interest in the application of composite materials in the infrastructure sector has begun a more rigorous approach in the evaluation of these materials to ensure that they perform within expected hygro-thermal-mechanical environment. The absence of significant data characterizing the long-term durability of glass fiber-reinforced polymeric composites and the absence of adequate established standards for the repair, design, and maintenance of glass fiber-reinforced composite have been the mitigating factors against the introduction of composites to industry. In order to circumvent the restrictions imposed by the absence of long-term data, simulation and other stochastic methods have been envisioned. These simulations provide insights into the long-term response of glass fiber-reinforced composite materials or their constituents to combined environments. The lack of long-term data is

not only restricted to the physical response of composite materials in the application environment but also the environmental and chemical synergism responsible for the premature failure of glass fiber-reinforced composite materials. Another salient advantage of a reliable simulation technique is that it allows for the establishment of performance bounds for the material. Performance bounds are essential because even though we may know the mechanics of environ-mechanical degradation and can describe it, we still have no predictive way of assessing the mechanical and environmental loading (severity and sequence) that the application environment will impose. Thus, the path-dependent damage process that the composite experiences will never fully allow one precise assessment of the remaining strength and life.

1.3 Objectives

This thesis focuses on the development of a micromechanics-based life prediction model for predicting the creep rupture and fatigue behavior of high performance glass fiber-reinforced polymeric composites by assimilating the Local Load Sharing model developed by Curtin et al. [8] and a fracture mechanics based time-dependant crack growth model. The simulated creep rupture and fatigue model will be compared to existing data. An attempt will be made to substantiate Mandell's stipulation [9-13]. That is, the slope of applied stress versus life is 10%UTS/decade, and it is independent of fiber orientation, fiber volume fraction, and resin type, and glass fiber type. This model will provide a further tool for the prediction of glass fiber-reinforced composite behavior in the absence of substantial experimental data.

Chapter 2 : LITERATURE REVIEW

2.1 Literature Review

This review looks at the durability factors that impede adaptation of composite material to civil and marine application. It delineates the role of moisture degradation, stress corrosion and glass fiber fatigue on the durability of fiber-reinforced composite materials (FRC). Since the durability of composite is heavily dependent on the durability of the fiber, the effect of stress corrosion on glass fiber-reinforced composites will be discussed. Significant attempts at reducing stress corrosion in glass fiber reinforced composites will be mentioned. Fatigue effect on glass reinforced composites and significant research in this area will be mentioned as a prelude to developing a micromechanics base model for characterizing the fatigue behavior and creep rupture of high performance polymeric composites. Mandell's work and other glass fiber fatigue related literature will be highlighted. Fracture mechanics based models such as those by Wiederhorn [14] and Ritter [15], for characterizing glass fracture will be mentioned. The numerical local load-sharing model for characterizing stress transfer among broken fibers will be mentioned, and the McCartney [53] statistical failure model will be cited.

2.2 Moisture Effect on Fiber-Reinforced Composites

The complete mechanisms involved in the degradation of composites under

humid environments are still under intense study. Moisture in many of its forms-acidic, basic, neutral are known to affect the durability of composites [19]. The corrosion of glass fibers, the dissolution of soluble compounds in matrices, increased interlaminar stresses, and the reduction in strength and modulus are moisture-related events that affect composite materials durability and damage tolerance [19].

2.2.1 Factors Affecting Moisture Absorption in FRC

Moisture absorption in composite materials is influenced by many factors. The nature and distribution of voids in composite materials dictate the volume of moisture it can retain. The presence of voids in the composite also has the effect of increasing the equilibrium moisture concentration and the diffusion coefficient. In most cases fiber diffusivity is negligible as compared to that of the matrix; however certain fibers such as Kevlar are known to absorb significant amounts of moisture [16]. Resin type is essential in the characterization of moisture absorption in composite materials, since moisture absorption is mostly a resin-dependent phenomenon. Certain resins such as epoxies are known to absorb moisture under different factors depending on their chemical structure. Typically, vinyl ester resins possess lower maximum moisture content than epoxy matrix resins. Moisture diffusion is known to be temperature dependent. The famous Arrhenuis equation incorporates this dependence:

$$D_z = D_{z0} \exp\left(-\frac{E}{RT}\right) \qquad (2.1)$$

Where:

E = activation energy (cal/g-mol)

R = universal gas constant (1.987 cal/g-mol-K)

T = absolute temperature (K)

D_{z0} = Diffusion coefficient (mm^2/sec)

Gillat and Broutman [20] have investigated the effect of stress levels on moisture absorption for T-300 carbon epoxy cross-ply. In these studies, the laminates exhibited higher coefficients of diffusivity with increasing stress levels; however the equilibrium moisture content was not affected [20]. Micro-cracks in composites allow the absorption of more moisture due to the capillary action of the voids; leaching through these voids might decrease moisture retention [20]. Thermal spikes affect the moisture absorption or desorption capabilities of composites. Adamson [21] speculated that thermal spike damage might be due to the nucleation of micro cracks at the fiber/matrix interface. Reverse thermal effect is a phenomenon that is characteristic of certain composite materials, where the composite exhibits a rapid increase in moisture absorption when ambient conditions such as temperature are suddenly reduced [21]. The volumetric changes associated with moisture absorption affect the physical properties such as strength of composite materials. This effect is manifested in the form of plasticization resulting from moisture absorption, the emergence of microcracks at the fiber/matrix interface due to moisture-induced residual stresses, or a combination of plasticization and interface degradation [21]. Volumetric changes can be computed as follows:

$$\varepsilon_m = \frac{1}{3}\frac{\Delta V}{V_o} = \frac{1}{3}\frac{\rho_m}{\rho_w} M = \beta_m M \qquad (2.2)$$

Where:

ρ_m = matrix density

ρ_w = water density

M = moisture content at time, t

The corresponding volumetric strain is given by,

$$\beta_m = \frac{1}{3}\frac{\rho_m}{\rho_w} \qquad (2.3)$$

where:

β_m is known as the swelling coefficient.

The dilatation due to moisture ingression is given by

$$\varepsilon_m = \varepsilon_1 + \varepsilon_2 + \varepsilon_3 \qquad (2.4a)$$

In most practical situations this swelling phenomenon is neglected until a certain moisture concentration threshold M_0 is exceeded. In that case the dilatation strain is given by:

$$\varepsilon_m = 0 \text{ for } M < M_0 \qquad (2.4b)$$

$$\varepsilon_m = \beta_m (M - M_o) \text{ for } M > M_0 \qquad (2.5)$$

Where:

M_0 is the amount of water absorbed in the free volume.

The study of moisture absorption characteristics of composites is of paramount importance in establishing *a priori* the performance of composites under marine conditions. In the marine industry ships are exposed to both wave action and the corroding effect of seawater. Hofer et al. [22] noted that stress cycling is predominant in the marine environment and that ships may be exposed to 10^7-10^8 cycles as a result of wave forces. Hayes et al. [23] noted that despite the prolonged processes involved in moisture ingression into composite materials, its repercussions outweighs that of temperature effects.

Moisture absorption studies by Shanker et al. [24] on glass/epoxy composites comprising alternate layers of CSM (continuous stranded mat) and WR (woven, roving) E-glass provided these salient points: that these systems are characterizable by Fickian diffusion process, that higher diffusivities were observed in the composite system with outer layers of CSM and, that for systems containing no CSM layers diffusivity was considerably less, indicating the hydrophilic nature of CSM, that diffusion does not change with from theoretical computations, and that equilibrium moisture level decreases with increasing WR (woven roving) volume fraction and vice versa.

2.3 Environmental Stress Corrosion in Glass-Reinforced Plastics

In spite of their attractive features such as tailorability and high strength, GRP is susceptible to the corrosive effects of the service environment although less so than steel. The combined effects of applied stress or strain and the hostile environment accelerate the degradation of GRP. Corrosion in GRP can be categorized as stress corrosion cracking if a constant stress is applied to the mechanical structure in the immersed state or strain corrosion cracking if the applied stimulus is strain [25]. Stress corrosion may be referred to as the mechanical and chemical degradation of FRC accelerated by the presence of hostile aqueous environment. This phenomenon is characterized by the spontaneous cracking of exposed single fibers to dilute acids, or the multiple cracking of composite laminates under applied stress [26,27]. Price et al. [28] agree that spontaneous fractures of glass fibers occur even in the absence of applied stress, and that the process involves two major stages namely: ion exchange phase and the leaching of glass surface phase. Both phases produce significant dimensional changes, which generate surface stresses locally on the fibers resulting in premature failure.

Hogg et al. [29] noted that the mechanism of crack growth in glass fiber composite materials under acid environments is still underdevelopment, but that the general observable trends in fracture development and failure are affected by:

- The fiber orientation density
- The angle between the principal stresses and principal fiber orientation

- Laminate arrangement
- The relative strengths of laminate constituents (fiber, matrix, fiber-matrix interface)

2.3.1 Fractography of FRP in Corrosive Environment

Scanning Electron Microscopy (SEM) and other optical apparatus provide evidence of stress corrosion of glass fibers in hostile environment. Figure 2.1 shows SEM of E-glass fibers after exposure to 25% H_2SO_4 for 4½ days. The vitriolic effect of 25% H_2SO_4 on the glass fiber is evident on the fiber surface, which is characterized by the peeling off of glass flakes and circular regions of material loss. Figure 2.2 shows SEM E-glass that has been exposed to 1N HNO_3. The helical crack patterns shows the corrosive effect of 1N HNO_3 to E-glass fibers.

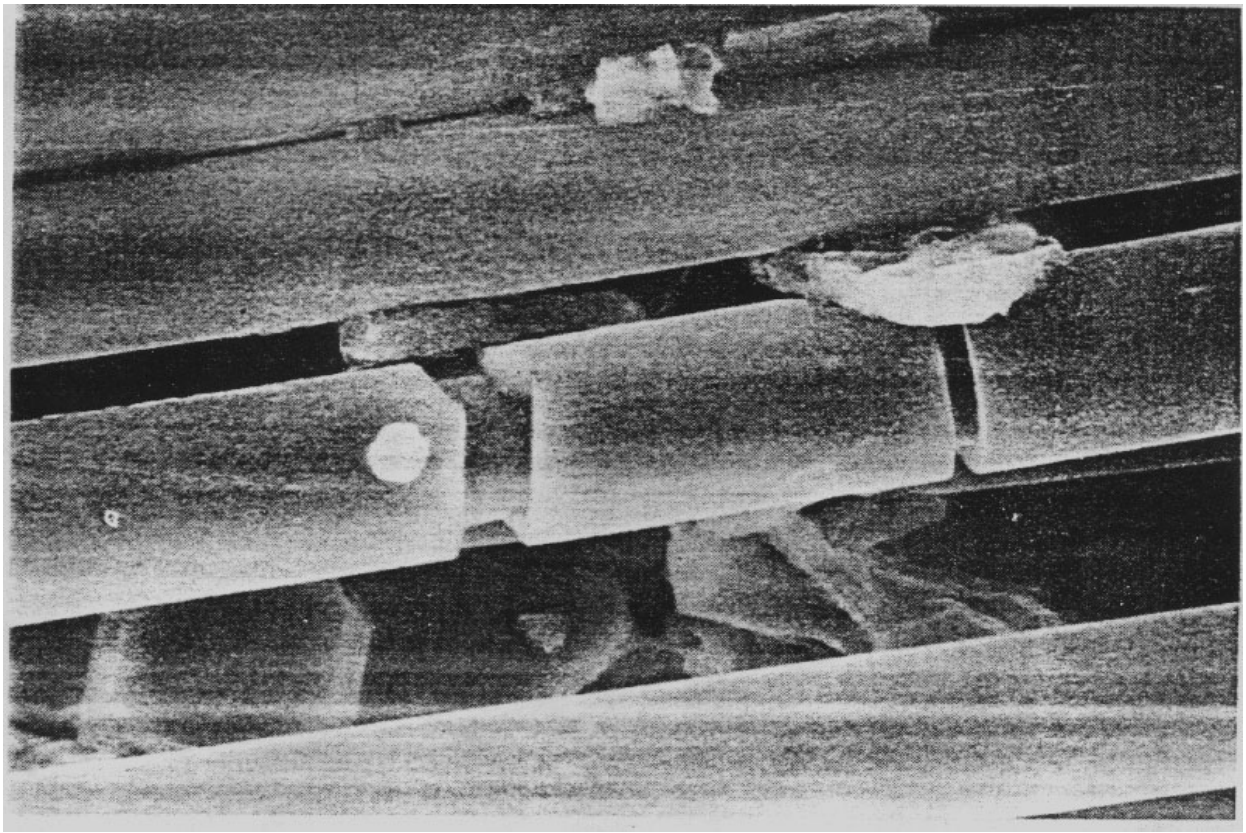

Figure 2.1: SEM of E-glass fibers after exposure to 25% H_2SO_4 for 4½ days (25).

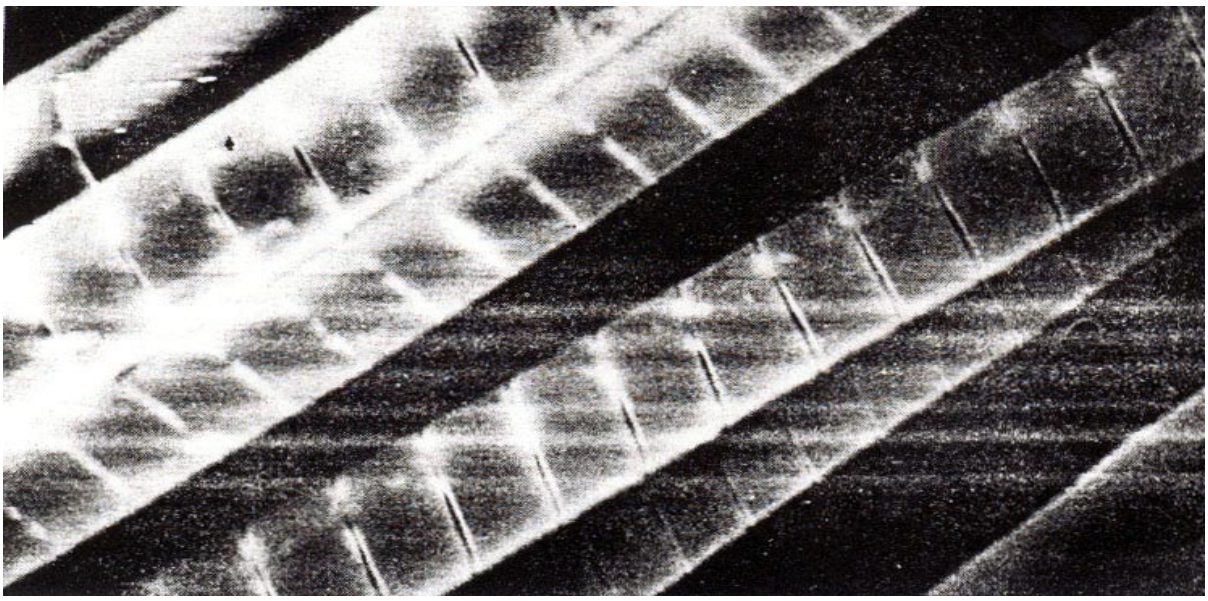

Figure 2.2: SEM of E-glass fibers showing helical crack patterns after exposure to 1N HNO_3 (25)

2.3.2 Attempts to Circumvent Stress Corrosion

2.3.2.1 Modified Fiber Approach

Numerous attempts have been made to eliminate or alleviate the effect of stress corrosion in FRP structures. Since fibers are the major victims of stress corrosion degradation, significant work have been done to find substitute fibers. For instance E-CR, a derivative of E-glass, has been found to withstand stress corrosion crack growth much better than the parent E-glass fiber [29]. E-CR glass and AR glass were found to exhibit considerable resistance to stress corrosion over standard E-glass and they both

do not form the characteristic helical cracked skin associated with E-glass in acidic environment [29] as shown on Figure 2.2.

2.3.2.2 Matrix Toughness Approach

Increased matrix toughness is another approach that has been taken lately to combat the menace of stress corrosion. Since the matrix provides the protective shield for the fiber against incursion by the environment, judicious selection of the matrix for a particular environment will offset the effects of stress corrosion failure. By increasing matrix toughness the rate of stress corrosion crack propagation in aligned GRP was reduced. It has also been documented that increased matrix toughness seems to reduce the stress concentration at the crack tip of the fiber resulting in increased time-to-failure of the fiber. However, this is not the case for brittle matrix [27].

2.3.2.3 Barrier Layer Approach

Barrier layers slow or prevent moisture ingression into structural laminates. Barrier layers come in the forms of thermoplastic sheets. Regester [30] studied the ingression of sulfuric acid, distilled water, HCL and NaCl solutions at different temperatures. He concluded that water ingression reduces flexural strength of laminates, and that this reduction is proportional to the amount of water sipping into the laminates and it is independent of time. Regester observed that neither HCL nor

sulfuric acid could ingress fully into the laminates even after 6 months at 100°C, and NaCl even penetrated less. Regester reached the conclusion that the sulfate ions ingress into the fiber-matrix interface by wicking and that the Na ions are readily polarized resulting in increased ionic radius, and thus decreasing diffusion [29,30].

2.4 Fatigue of Glass Fiber-Reinforced Composites

2.4.1 Fatigue Frequency Effect

Studies on fatigue frequency effect on composites have been inconclusive as a result of variant experimental results. Some fatigue frequency investigations have shown that higher frequencies produced higher cycles-to-failure, other works have shown the converse. Mandell and Meier, using a square wave, studied load frequency effects for cross-ply E-glass/epoxy laminates [33,34]. Using 0.01, 0.1, and 1 Hz frequencies, they observed that the number of cycles increased with increasing load frequency. Sendekyj and Stanaker made similar observations when they tested quasi-isotropic T300/5208 laminates at two frequencies, 0.167 and 0.0167 Hz respectively. In order to minimize strain effects a trapezoidal load shape was used in these analysis and failure times increased with increased frequency. Rotem, however, observed 10 times decreased in fatigue life when the frequency increased from 2.8 to 10 Hz for a quasi-isotropic T300/934 graphite/epoxy laminates at R=-1.0. Rotem attributed the decrease in fatigue life to hysterisis heating at the free edges [34,35].

Demers [40] as shown on Table 2.1, has evaluated fatigue frequency effect on specimen heating during cycling for E-glass fiber system. Figures in Table 2.1 indicate a change in temperature up to about 24°C at 3Hz and 60% UTS. Similar studies by McBagonluri et al. [42] did not show this trend for E-glass/vinyl ester. In fact the rise in temperature did not exceed 5°C and there was no significant heating between 2 and 10 Hz respectively [42].

Table 2.1: Fatigue Frequency Effect on Specimens heating (37)

$\sigma_{max}/\sigma_{ult}$	R	Frequency (Hz)	Max ΔT (°C)[a]
0.8	0.1	1	8
0.8	0.1	3	11
0.8	0.1	5	11
0.8	0.5	3,5	3
0.6	0.05, 0.1	1	8
0.6	0.1	3	24
0.6	0.1	5	21
0.6	0.5	3	5
0.6	0.5	5	4
0.4	0.1	5	12
0.4	0.5	5	1

2.4.2 Tensile Fatigue of Composites: Fiber-Dominated Mechanism.

Mandell [9] notes that fatigue failure, in general, is characterized by the progressive accumulation of cracks in the matrix and at the interface, resulting in loss of remaining strength and stiffness. This progression in remaining strength values reach a limiting point where it equals the cyclic stress and, consequently, failure results. This general trend in failure does not explicitly apply to tensile failure in glass-reinforced composites, where failure appear to be either a fiber- or a strand-dominated

phenomenon, and it is independent of matrix type or interface. Mandell stated that this damage mechanism for fiber-reinforced composites were true for cyclic as well as static fatigue, and that the stress levels versus cycles-to-failure curve properties is translated into withstanding crack initiation and progression. Mandell, however, cautions that exceptions to the fiber-dominated mechanism may exist when a severe fatigue mechanism is at play especially in woven fabric reinforcement and in very ductile matrices [9,10].

Mandell investigated the S-N curve behavior of three different fiber-reinforced composites namely: 0°/90° unidirectional ply glass/epoxy, injection-molded glass/polycarbonate, and SMC. The fiber architecture comprised of continuous fiber (V_f = 0.5), very short, partially oriented fiber (V_f = 0.24), and a chopped long randomly oriented strand of about 5 cm long and with volume fraction of 0.15. By fitting the data to equation 2.6

$$\frac{\sigma}{\sigma_{ult}} = 1 - \frac{B}{\sigma_{ult}} LogN_f \qquad (2.6)$$

Where:

σ = maximum cyclic tensile stress

σ_{ult} = ultimate tensile strength (UTS)

N_f = life

B = constant

Mandell obtained the slopes, B/UTS. The inverse of the slope of equation 2.6 (the fractional drop in tensile strength per decade cycles) were obtained as 9.8, 8.8 and

10.5 which were all close to 10. All the materials in Table 2.2 exhibited S-N curves similar to these results with R = 0.0-1.0. Table 2.3 gives the summary of the fit of equation 2.6 to various strand composites. It is interesting to note that the rate of strength lost is nearly invariant. Mandell asserts that for tensile fatigue up to 10^6 or 10^7 cycles, the fibers dominate the failure mechanism and that it is independent of the matrix type, interface, void content, filler content, fiber content, and to a large extent dispersion in data and composite length [9-13]. Mandell concluded that, even in the presence of the aforementioned variables the characteristic slope of 10% UTS/decade is still consistent with the fatigue of glass fiber-reinforced composites.

Subsequent work by Sims and Gladman [37-38] substantiated considerably Mandell's stipulation. In their undertaking Sims and Gladman used a constant rate of stress application, and then normalized their results to the dynamic fracture stress. The curves of the normalized stress vs. log N for woven glass-epoxy laminate (V_f = 0.47), were found to coincide, *independent of pre-conditioning treatment, orientation of reinforcement, or preloading-induced mechanical damage*. These results validate to a large extent Mandell's postulate that fiber-dominated mechanism is responsible for final composite failure.

Jones et al. [39], following similar methods described by Sims et al., attempted to verify Mandell's model. Their fit for boiled GRP specimens using equation 2.6 gave a slope of 13 UTS/decade and that for the dry specimens, the slope was 8.7 UTS/decade. Although Jones et al. concluded that their model does not readily lay

credence to Mandell's assertion, it is arguable that the deviation of their results from the slope of 10 %UTS/decade proposed by Mandell is not substantial given the inherent variations in fatigue data at different applied stress levels. A deviation of 13% for the dry laminates and about 30% for the boiled may be acceptable as consistent with Mandell's by reason of inherent statistical variations in fatigue data.

Demers [40] has conducted extensive fatigue tests on fiber-reinforced polymeric composites for infrastructure applications. Demers' test matrix is shown in Table 2.4 with corresponding slopes from equation 2.6. Demers' data and the assigned 95% lower confidence fit tallies quite well with Mandell's as shown in Table 2.3. Demers obtained a slope of 0.077 for the lower confidence fit, which is about 13% UTS/decade, 30% higher than Mandell's, but the scatter in the data could be responsible for this slight discrepancy. Another possible reason is that the 95% confidence level fit does not seem to match the general trend in data flow [40].

Table 2.2: E-glass Reinforced Composites of Different Matrices, Fiber Type and Volume fraction (9)

Description	Matrix	Nominal fiber volume fraction
Unidirectional	Epoxy	0.50
Unidirectional	Epoxy	0.33
Unidirectional	Epoxy	0.16
0°/90°	Epoxy	0.50
Injection molded	Nylon 66	0.23
Injection molded	Polycarbonate	0.24
Injection molded	Polyphenylene sulphide	0.25
Injection molded	Poly (amide-imide)	0.19
Chopped strand mat	Polyester	0.29
SMC (.64x.64x.32cm)	Filled Polyester	0.15
(25x.64x.32cm)	Filled Polyester	0.15
SMC-R50	Filled Polyester	0.35
$[0°/\pm45°/90°]_s$	Epoxy	0.50
Chopped strand mat	Polyester	0.20
impregnated strand	Polyester	0.23
impregnated strand	Epoxy	0.45
impregnated strand	Toughened epoxy	0.49
unimpregnated strand	None	1.00

Table 2.3: S-N Curve Parameters for Strand Tests (9)

Matrix	V_f	UTS (MPa)	UTS/V_f (MPa)	UTS/ B
Unimpregnated	1.0	1530	1530	11.0
unimpregnated strand (cleaned strands)	1.0	1219	1219	11.0
Polyester	0.23	455	1980	10.0
Epoxy	0.45	971	2160	11.0
Rubber-modified	0.49	1102	2250	10.4
Epoxy unimpregnated	1.0	1426	1426	11.6

Table 2.4: Demers' Fatigue data for Glass Fiber-Reinforced Composite (40).

Composite	B/UTS	UTS/B
unidirectional continuous	0.0978	10.2
0°/90° continuous	0.0856	11.6
±45 continuous	0.1440	7.0
Weave continuous	0.0755	13.2
short fiber[1]	0.1136	8.8
short fiber[2]	0.0604	14.5
Unidirectional continuous mat[3]	0.1079	9.3
unidirectional continuous mat[4]	0.0769	13
95% Lower Confidence	0.0775	13

[1] isotropic
[2] anisotropic
[3] R<=0.1 E-glass/vinyl ester
[4]R>0.1E-glass/vinyl ester

2.4.3 Fatigue Crack Growth in Fiber-Reinforced Composites

2.4.3.1 Background: Crack Growth in Glass Fibers

Numerous theories based on fracture mechanics have been developed or advanced to characterize the failure of glass fibers or glass fiber-reinforced composite. These theories and their resulting models have come about as a result of the complexity involved in the modeling of strength, fatigue and creep rupture performance of glass fibers, and consequently, glass fiber-reinforced composites. Glass composition, nature of mechanical damage (intrinsic flaw), load-time function, environmental media and temperature influence glass fiber strength as well as its fatigue and creep performance. The interaction of one or more of these factors might lead to varying degrees of fiber response, which may not be easily represented by a single model. This interplay between multiple environmental and mechanistic factors have impeded the development of a singular unified and representative model for assessing the longevity of glass fibers or their derivatives in the application environment. The major assumptions underlying these models include delayed failure due to stress-enhanced growth of intrinsic flaws to critical dimensions resulting in catastrophic failure [18,34].

The existence of intrinsic and extrinsic flaws in glass fibers has been known to lead to failure of glass fiber and glass reinforced composites. Intrinsic flaws are known to exist even in pristine glass under various surface conditions and relative humidity.

Table 2.5 shows penny-shaped surface flaw data obtained for different glass fibers under different environmental conditions and surface treatments. It is evident from Table 2.5 that even in the untreated and pristine state glass fibers possess intrinsic flaws. It is thus, the interaction of the intrinsic flaws coupled with the extrinsic flaws that result in the deterioration of the load-bearing agents in fiber-reinforced composites during fatigue cycling.

In his studies of the fracture mechanics of glass fiber, Wiederhorn [14,49] noted that the crack velocity is controlled by the rate of chemical reaction at the crack tip and the radius of the crack curvature is constant as crack progresses. The assumption that the failure of glass is the result of stress-dependent growth of intrinsic flaws rising to critical dimensions for spontaneous cracking to occur, is the basis of the fracture mechanics of glass fibers [49].

Table 2.5: Flaw size of some typical fibers (16-18, 43-47).

Glass	Surface Treatment	Test condition (%RH)	Median Inert Strength (MPa)	Flaw size (m)
Soda-lime-silica	Abraded	Wet	73-150	$1.7\text{-}7.3 \times 10^{-5}$
	Acid-polished	50 &100	3242	3.7×10^{-8}
Borosilicate	Abraded	100	125	2.3×10^{-5}
	Acid-polished	100	2866	4.5×10^{-8}
Fused Silica	Abraded	50	104	3.9×10^{-5}
	Pristine fiber	100	41,055	2.1×10^{-9}
E-glass	Pristine fiber	50	5650	1.5×10^{-8}
Optical Glass[1]	Coated pristine fiber	97	6760	9.2×10^{-9}
Optical Glass[2]	Coated pristine fiber	55	5620	1.3×10^{-8}
Optical Glass[3]	Coated pristine fiber	16	5945	1.2×10^{-8}

[1]Germanium doped fused silica core with fused silica cladding and polyurethane coating
[2]Fused Silica core with Hytrel plastic coating
[3] Germanium doped fused silica core with borosilicate cladding & Hytrel plastic coating

Wiederhorn noted that the crack velocity can be represented as by a power function

$$V = ax_o^f e^{\left(\frac{-E^*}{RT}\right)} e^{\left(\frac{bK_I}{RT}\right)} \tag{2.7}$$

where:

x_o = partial pressure of H_2O

f = order of chemical reaction

E^* = empirical measurement of zero stress

R = gas constant

T = thermodynamic temperature

K_I = stress intensity factor

a, b = constants

For a specific stress level, temperature, and humidity history (2.7) can be integrated to give

$$t_r = \frac{2K_{IC}^2}{AY^2 n\sigma_a^2}\left[\frac{\sigma_a}{S_i} + \frac{1}{n}\right] e^{-n\frac{\sigma_a}{S_i}} \tag{2.8}$$

Where:

$$A = ax_o^f e^{-\frac{E^*}{RT}} \tag{2.9}$$

and

$$n = \frac{bK_{IC}}{RT} \tag{2.10}$$

where:

S_i= inert strength (the strength determined in an environment in which no subcritical crack growth occurs).

K_{IC} = critical stress intensity factor

Y= flaw shape factor

According to Ritter [15] equation 2.7 requires numerical solution for a constant stressing rate. Thus, numerical integration must be employed for a given constant stress level, σ. Wiederhorn obtained such a closed form solution in [14].

$$\int_{\frac{K_{IC}\dot{\sigma}}{S_i}}^{\frac{K_{IC}\dot{\sigma}}{\sigma_f}} \frac{K_I}{t} d\left(\frac{K_I}{t}\right) = \frac{Y^2 \dot{\sigma}^2 A}{2} \int_0^{t_f} e^{nK_I} dt \tag{2.11}$$

Where:

σ_f = fracture strength

K_{Ii} = initial stress intensity factor

σ (dot) = stressing rate (dynamic stress)

A= constant

Y = geometric parameter

The fatigue constants A and n can be obtained as functions of temperature and humidity by regression analysis of constant stress or stressing rate data obtained from

experimental data at various temperatures and humidities from equations (2.8) through (2.11). Table 2.6 shows values obtained using regression analysis techniques. These parameters are essential in modeling glass fiber mechanics and degradation.

Non-regression techniques using computer search methods have previously been undertaken to obtain values for the constants in equation 2.9-2.10 as depicted on Table 2.7. In this case, however, f is held constant while the other parameters are sought [15]. Analysis from the resulting temperature and partial pressure dependence of A and n can be utilized to obtain the stress free activation energy E^*, the order of reaction f, and the constants a and b.

Table 2.6: Summary of Stress Corrosion constants based on Fatigue data of Optical Glass Fibers (18)

E^*(kJ/mol)	b($m^{5/2}$/mol)	f	Type of fatigue data	Ref
109 to 231	0.318 to 0.488	-0.5 to 0.9	Static	18
55 to 92	0.435 to 0.572	-0.8 to 0.5	Dynamic	50
29	-0.101	-	Static	52 (high stresses)
378	1.05	-	static	52 (low stresses)

Table 2.7 Summary of Stress Corrosion Constants Based on fixing f Equal to One & Averaging N Values over Humidity at Each Temperature (18)

E^* (kJ/mol)	B($m^{5/2}$/mol)	f	Ref
-0.291	0.124	1	18
55	0.200	1	50

2.4.3.2 Contribution of Glass Fiber Composition

Ritter derives an approximate static fatigue model from the universal fatigue curve given in equation (2.8).

$$\frac{\sigma_a}{S_i} = 0.5 - \frac{1}{n}\ln\frac{t_f}{t_{0.5}} \tag{2.12}$$

t_f = failure time at an applied stress equal to half the inert strength

n = compositional parameter

The parameter n is a source of contention. Many authors argue that the value of n obtained from the fatigue model is a compositional parameter, which is related to stress corrosion reaction on glass. On the other hand static fatigue data indicate that n depends on the surface conditions [18]. This parameter is essential since it is an input to the micromechanics model in the chapter 5 of this thesis. Ritter attributes the disparity in n values for uncoated silicates in the fatigue and stress corrosion cases as an indication that a mechanism other than the development of subcritical crack growth of intrinsic flaws is responsible for failure [18].

2.4.3.3 Contribution of Temperature and Humidity

The effect of temperature and relative humidity on the performance of glass-reinforced composites is phenomenal. The constituents of glass are known to degrade under prolonged exposure to environment. Stress corrosion factors are accelerated by the coupled effect of temperature and moisture as elucidate in sections 2.1-2.3. The dependence of moisture and temperature diffusivity is represented by Arrhenius relationship. Ritter [18] expresses the moisture and temperature relationship as follows:

$$\ln A = \ln a + f \ln x_o - \frac{E^*}{RT} \tag{2.13}$$

The slope of the plot of 2.13 (ln A vs. In x_o) indicate different slopes values (0.8-0.5) for different temperatures. These apparent differences in slope were attributed to change in stress corrosion mechanism [18].

Using similar techniques as Wiederhorn [14], Ritter [15] derived a detailed fracture mechanics-based static model for glass fiber as follows:

The stress intensity factor at a given flaw size, a is given by

$$K_I = \sigma_a Y \sqrt{a} \tag{2.14}$$

where:

Y = geometry of the flaw

σ_a = constant applied stress

by taking the derivative of 2.14 with respect to time we obtain 2.15

$$\frac{dK_I}{dt} = \left(\frac{\sigma_a{}^2 Y^2}{2K_I} \right) V \tag{2.15}$$

where V = crack velocity. By separating variables and integrating from an initial stress intensity factor K_{Ii} (at the most critical flaw) to a critical intensity factor K_{IC} we obtain 2.16

$$t_r = \int_{K_{Ii}}^{K_{IC}} \frac{2}{\sigma_a{}^2 Y^2} \left(\frac{K_I}{V} \right) dK_I \tag{2.16}$$

Expressing the crack velocity as a power function of K_{Ii}

$$V = AK_I^N \tag{2.17}$$

where A and N are constants. By substituting 2.17 into 2.16 we obtain 2.18

$$t_f = \left[\frac{2}{AY^2 (N-2)\sigma_a^2} \right] K_{Ii}^{2-N} \tag{2.18}$$

Ritter discarded the term K_{IC}^{2-N} with respect to K_{Ii}^{2-N} since for a glass fiber $10 < N < 50$ and for normal service condition the stress is in the range $K_{Ii} < 0.9 < K_{IC}$ [15,18]. By taking advantage of the linear relationship between the stress intensity factor and the applied stress, the initial intensity factor can be expressed as

$$K_{Ii} = \frac{(\sigma_a / S_i)}{K_{IC}} \tag{2.19}$$

where:

S_i = fracture strength in an inert environment.

The substitution of 2.19 into 2.18 result

$$t_f = \left[\frac{2}{AY^2(N-2)K_{IC}^{N-2}}\right] S_i^{N-2} \sigma_a^{-N} \tag{2.20}$$

Equation 2.20 represents the time require for the initial flaw to grow from a subcritical size to critical dimensions required for failure to occur. The term in bracket is a constant for a given glass, and for a given test conditions.

2.5 Statistical Modeling of Failure of Fiber-Reinforced Composites

2.5.1 Curtin's Lattice Green Function Model

The lattice Green function model is a numerical model for investigating the tensile failure of unidirectional fiber reinforced composites. It makes use of 3-D lattice Green's functions to compute load transfer from broken to unbroken fibers by also including the effect the fiber/matrix sliding. By incorporating a spatial parameter, the nature of the load transfer can be altered. This model, in addition to the residual model, serves as the basis for the simulation model developed in this thesis. The detailed derivation of Curtin's model is shown in [8].

2.5.2 McCartney's Corrosive Environment Model

McCartney [50] considered the effects of corrosive environment and constant applied stress on the large bundle of loose fibers. This model stipulates that stress corrosion mechanisms are responsible for the time-dependant growth of surface defects in fibers. These mechanisms, he argues, result in the eventual catastrophic

failure of the fiber bundle. Using the premise that the time-dependant bundle strength is related to the initial defect size distribution and using a defect growth model, McCartney related bundle strength to the flaw size and flaw distribution in the bundle of fibers. Some of McCartney assumptions where as follows:

- Fiber exhibit linear elastic behavior even near complete failure.
- Uniaxial stress in fiber is extension-dependant
- Uniaxial stress in fiber is independent of rate of load application
- Applied load is shared equally among surviving fibers
- Twisting effects are negligible
- Strength distribution of fibers may be represented by a Weibull distribution or any other statistical distribution.

McCartney's approach embodies some of the salient procedure implement by Curtin et al. which is the subject of Chapter 5.

Chapter 3 : EXPERIMENTAL PROCEDURES

3.1 Material System: Composite Panel

In this undertaking composites consisting of vinyl ester resin reinforced with E-glass random CSM sandwiched between 0° E-glass roving were aged in 3.5% NaCl solution at 65°C. A sketch of the fiber arrangement is as shown in Figure 3.1. The manufacturer (Strongwell Inc.), for this material system has reported a volume fraction between 28-30% fiber, obtained by matrix combustion. In this study, coupons of dimensions 9''(22.9 cm) long x 1/8''(0.32 cm) thick x 1''(2.54 cm) were cut from the plate using a wet diamond blade. The dimensions of the plates were 1/8''(0.32 cm) thick x 18''(40.6 cm) long x 48''(122 cm) wide [55-57]. The specimens' edges were sanded to ensure uniformity and also to avert premature failures due edge defects.

Figure 3.1: EXTREN™ Laminate Showing Fiber Arrangement

3.2 Specimens Preparation for aging

The cut edges of the specimens were coated with a two-part epoxy and cured at 50°C for 2 hours. The specimens were individually weighed before insertion into an aging tank. Specimens were arranged in a plexiglass rack to insure equal and maximum exposure of each specimen to the 3.5% NaCl solution. Figure 3.2 shows a

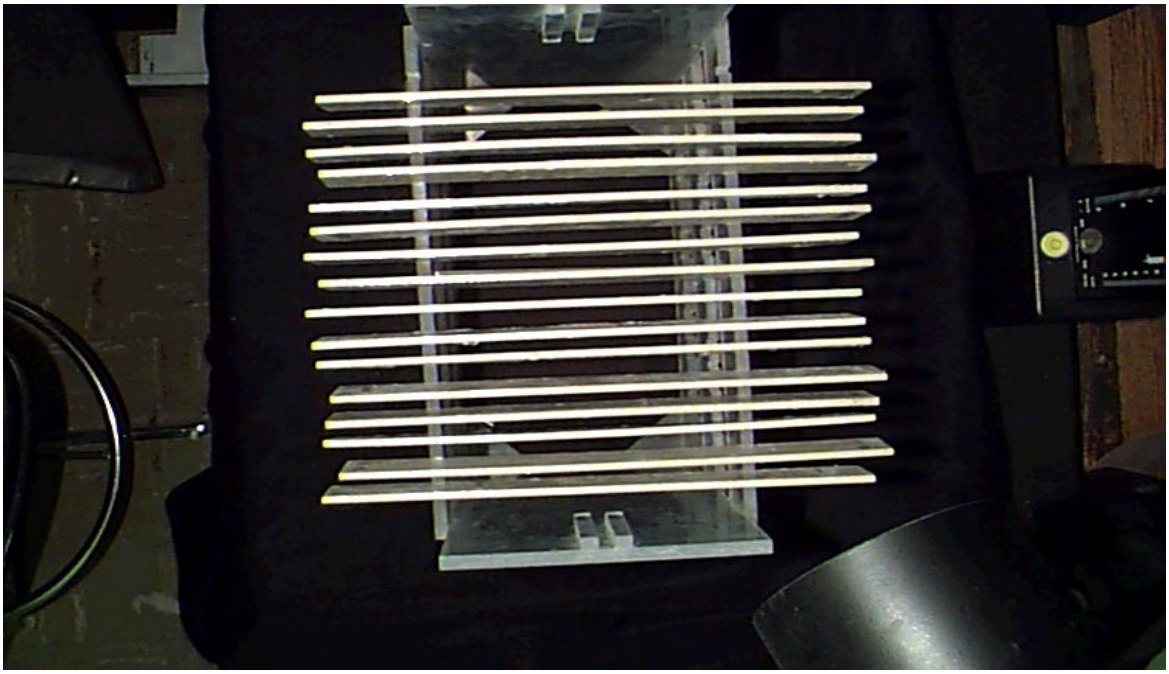

Figure 3.2: Racked Specimens ready for aging

set of specimens on a typical rack prior to immersion into an aging tank.

The amount of moisture uptake was determined in the specimens each day by quickly taking them out of the bath tank, wiping them dry, weighing them and then re-inserting them into the tank.

3.3 Solution preparation and Monitoring

The preparation of 3.5% NaCl solution required 3.5g of NaCl in 100g of water; 100g of water is equivalent to 100ml. A volumetric flask with a capacity of 2000ml was used to make the solution until the 20gal (75.7liters) tank was filled. To ensure that the concentration of salt was at the required concentration, a fresh solution was made for each batch of specimens. The salinity of the solution was monitored by a salimeter and adjusted periodically by adding fresh solution.

3.4 Aging procedure for specimens in 3.5% NaCl at 65°C

The setup consisted of a 20gal tank made up of transparent glass to facilitate experimental monitoring without disturbing the setup. Four aquarium heaters (auto-power) were mounted at the four corners of the tank. An Omega controller was used to maintain the temperature at 65°C. Two power pumps (powerHead 402 type manufactured by Hagen USA) were placed in the tank to ensure uniform heat distribution in the setup during aging. Custom-made racks with the capacity of approximately fifty specimens were designed to carry the specimens during aging as shown in Figure 3.2. Each specimen was allotted a groove to reduce any interaction with adjacent specimens and to allow for maximum exposure to the prevailing fluid condition as shown in Figure 3.2. Insulation and sealing of the tank was attempted to

reduce evaporation and heat loss.

Weight changes in the specimens were recorded daily and the percent weight gain computed as follows:

$$\%U_T = \frac{W2 - W1}{W1} \qquad (3.1)$$

Where:

W1 = dry weight

W2 = wet weight

$\%U_T$ = percent moisture uptake

3.5 Environmental Fatigue Fluid Cell

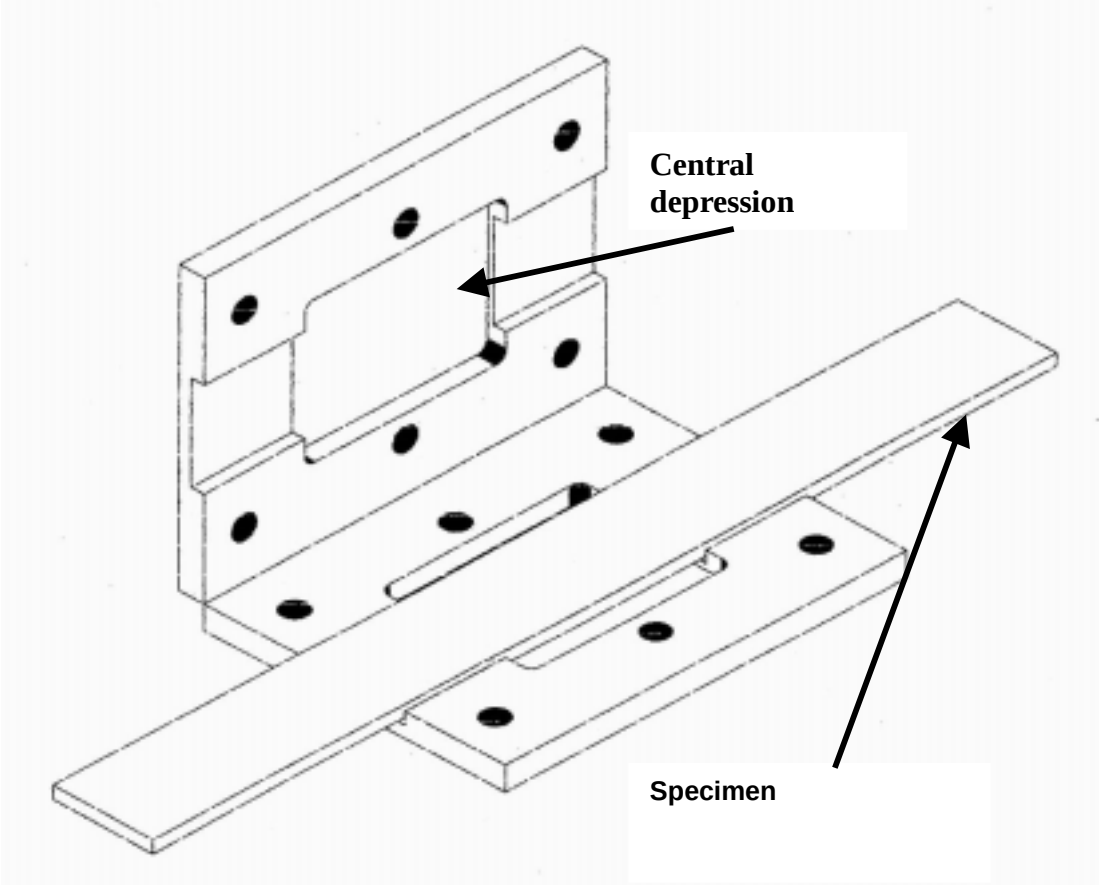

Figure 3.3: Environmental Fluid Cell Assembly

A transparent fluid cell was designed to carry NaCl solution around the specimens during testing. Figure 3.3 shows a typical fluid cell assembly. This cell has a groove on both plates and a central depression where fluid is momentarily sustained during testing. This depression encloses the gage section of the coupon. The fluid cell does not leak during cycling except upon failure; leaking is unavoidable when the specimen fails. The fluid cell covers about 4” of the mid-section of the specimens.

3.6 Specimens Preparation for Fatigue

A typical fatigue specimen was prepared by enclosing the central region of the specimen within the fluid cell (*see Figure 3.3*). The remaining equal lengths on either side of the fluid cell were used for gripping. A length of 0.5 inches was left between the cell and the grips of the MTS machine on either side of the cell. Thus, 2 inches of specimen length resided in the grips. Silicone was laid in beads along the edges of the depression in the center of the cell during cycling. In addition, six screws were used to fasten the two identical plates together, enclosing the mid-section of the specimen. Prepared specimens were stored in a cooler for about six hours to allow the silicone to cure, and to prevent moisture loss during curing.

3.7 Description of Testing

3.7.1 Quasi-static Tensile

The quasi-static properties of the material system were evaluated for each batch of pre-conditioned specimens. A screw driven Instron was used to evaluate the quasi-static strength and stiffness. An extensometer was used to acquire strain data and transverse and axial strains were obtained using CEA-13-125WT-350 strain gages. Gages were applied to the wet samples using M-bond 200 cynoacrylate adhesive without causing loss of moisture content. The specimens were tested at a 0.05 inches/min strain rate.

3.7.2 Fatigue: Tension-tension R = 0.1 at 30°C

In this undertaking the gripped ends of the specimens were wrapped with fine wire mesh to prevent slip in the grips during fatigue. The prepared specimen was then connected to the EX 211 circulator bath by means of polyurethane tubes. The temperature of the cell was maintained at 30°C by means of an adjusting knob and an attached thermometer. The appropriate stress levels were computed and inserted into the Testlink data acquisition system. The appropriate frequency was set and then the Ex 211 circulating system was turned on. The circulating fluid was allowed to equilibrate by ensuring that bubbles were not present before the initiation of the testing.

The NaCl solution for the fatigue process was made using the same techniques described in the solution preparation section. There was a drift of temperature to about 30.9°C, on the average, during the fatigue process, starting with an initial temperature of 30°C. This procedure was employed for testing at 2 and 10 Hz respectively. S-N curves were generated for the material system by cycling the coupons to failure and recording the number of cycles-to-failure. At a given stress level the residual properties of the material were evaluated by cycling the material to a preset number of cycles at given stress levels and then testing it quasi-statically on the screw-driven Instron. Stiffness was obtained at 10Hz by using an extended extensometer bridged across the fluid cell. All fatigue testing was done on a 10Kip MTS servo-hydraulic machine a sketch is shown in Figure 3.4.

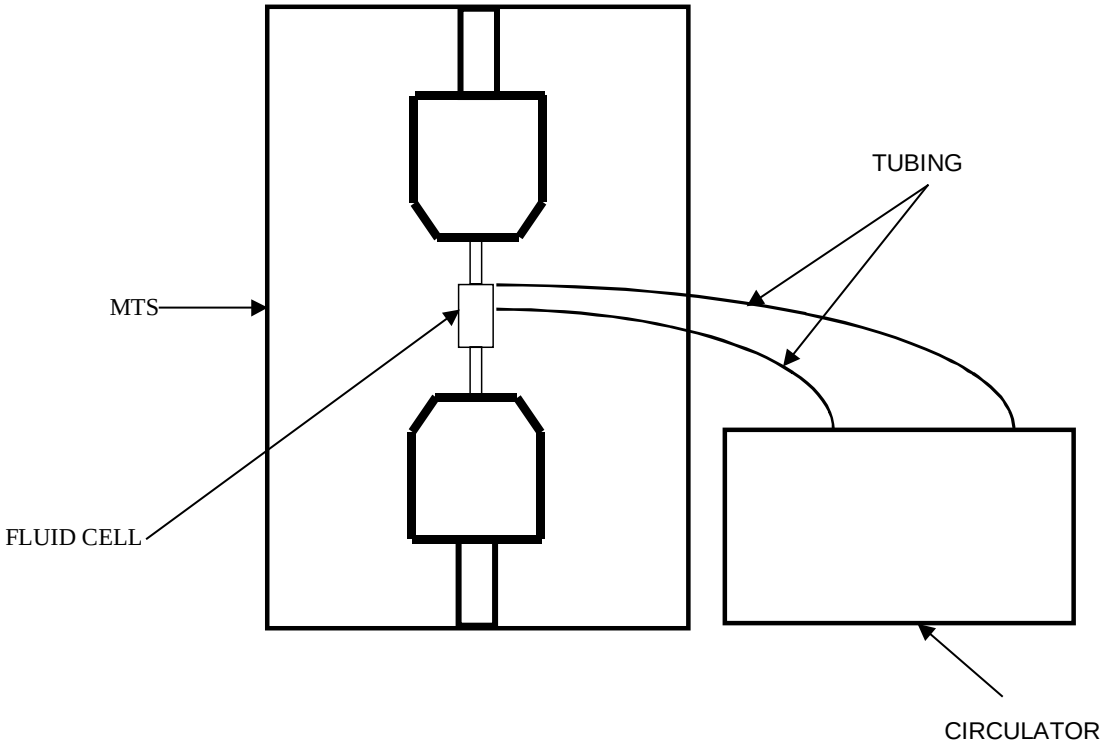

Figure 3.4: Setup for Fatigue Testing

3.7.3 Fatigue: Tension-tension R = 0.1 at 65°C

In this portion of the study specimens prepared by the procedures stated above (*under Fatigue: Tension-tension R = 0.1 at 30°C*) were employed. In this case however, the temperature of the simulated circulating seawater was elevated to 65°C. The heater in the Ex 211 circulator bath was set to 65°C. The heated simulated seawater was allowed to equilibrate by means of an attached thermometer i.e. the temperature of the fluid was stabilized at 65°C before the experiment was initiated. The experiment was then initiated. The heater was kept running in between specimens

replacement and the temperature checked before subsequent tests to ensure that the circulating fluid temperature was maintained.

Chapter 4 : RESULTS AND DISCUSSIONS

4.1 Dry Specimens

The quasi-static properties were evaluated for the as-received, salt-aged and water-aged EXTREN™ material system. Weibull statistics, which provides a more appropriate representation of the variation of laminate properties, was used to compute the average strength, modulus, and Poisson's ratio as well as the A and B allowable for the material strength [54]. These results are depicted in Table 4.1. Equations 4.1 through 4.3 through were used to compute the Weibull parameters. The Weibull parameters for the dry material were obtained using eleven specimens, and for the wet- and salt-aged specimens, fourteen specimens were used in each case. A normalized plot of the residual quasi-static properties is shown in Figure 4.1 with the corresponding standard deviation bars. The distribution of static strength properties does not seem to vary significantly in shape. The dimensionless shape parameter, α is constant for the three conditions, namely: as-received (dry), wet and salt.

Table 4.1: Quasi-Static Properties of EXTREN™-As-Received, Salt-Aged and Water-Aged.

	Parameters				
Medium	X	A Allowable (MPa)	B Allowable (MPa)	ν	E
Dry	212±20 MPa $\alpha = 13$ $\beta = 220$ MPa	149	179	0.31±0.03 $\alpha = 8.4$ $\beta = 0.34$	15.5±0.6 GPa $\alpha = 25$ $\beta = 15.8$ GPa
Wet	145±13 MPa $\alpha = 13$ $\beta = 151$ MPa	102	122	0.31±0.06 $\alpha = 5.4$ $\beta = 0.4$	14±1.3 GPa $\alpha = 12.5$ $\beta = 14$ GPa
Salt	144.7±13 MPa $\alpha = 13$ $\beta = 150$ MPa	100	121	0.32±0.04	13.8±3 GPa

$$P(\sigma) = 1 - e^{-\left(\frac{\sigma}{\beta}\right)^{\alpha}} \qquad (4.1)$$

Where:

α = dimensionless shape parameter

β = location parameter (MPa or psi)

P(σ) = probability of surviving stress

The corresponding mean and variance of the laminates are computed as follows:

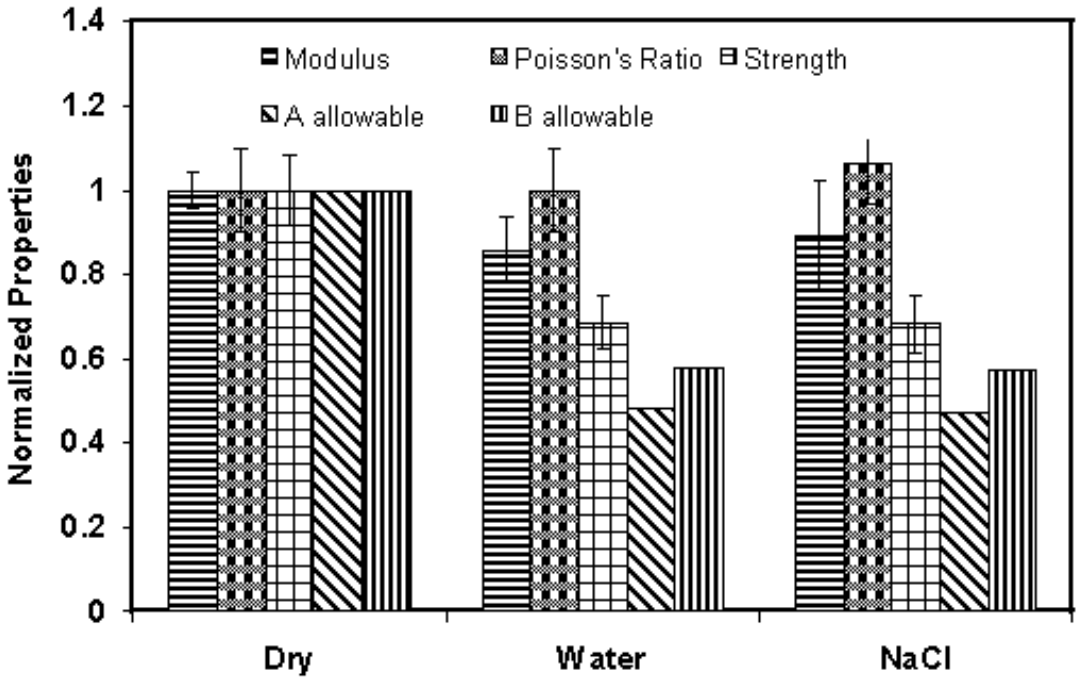

Figure 4.1: Normalized residual properties

$$\bar{\sigma} = \beta\Gamma\left(\frac{1+\alpha}{\alpha}\right) \tag{4.2}$$

$$s^2 = \beta^2\left[\left(\frac{2+\alpha}{\alpha}\right) - \Gamma^2\left(\frac{1+\alpha}{\alpha}\right)\right] \tag{4.3}$$

Where:

Γ = gamma function

s = variance

These results indicate that the quasi-static modulus underwent a change of 11% and the strength a reduction of 32%, from dry to NaCl-aged. The Poisson's Ratio increased by 6%. Data from the water-aged specimens indicate a decrease in modulus of about 11% and 32% in ultimate tensile strength respectively, from dry to water-aged. There was no change in Poisson's Ratio for this case.

4.2 Fatigue Curves

Fatigue curves for the glass/vinyl ester reinforced composite EXTREN™ indicate similar trends in slope independent of moisture exposure or content or type of moist environment as depicted in Figures 4.2 and 4.3. In other words the aged and the un-aged EXTREN™ undergoes a similar failure mechanism. Furthermore, Figure 4.2

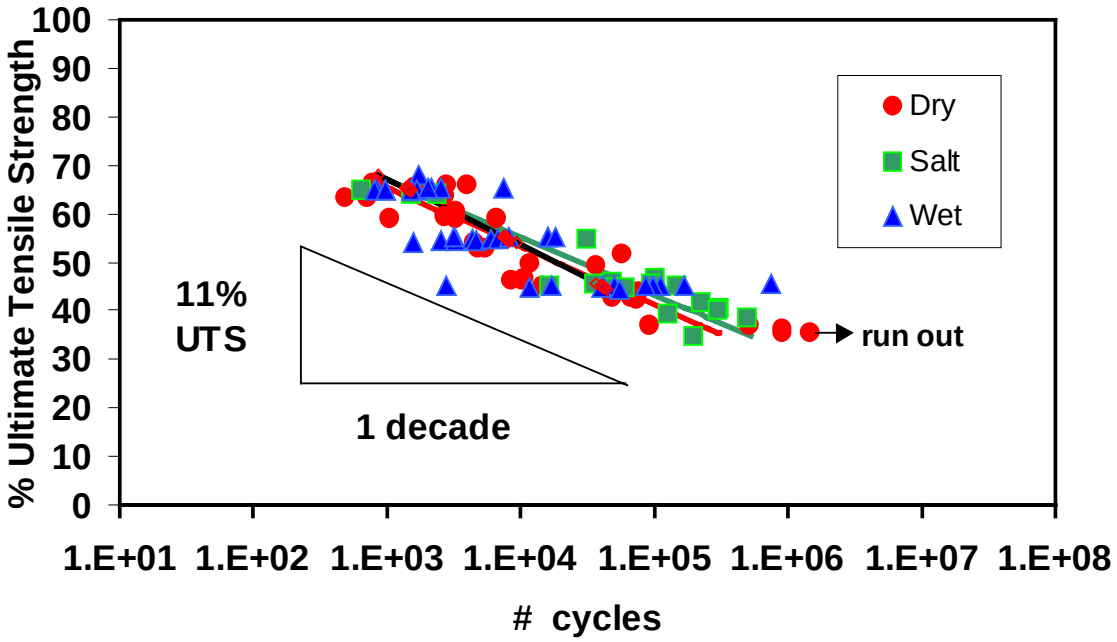

Figure 4.2: Normalized fatigue curves for dry, wet, saltwater-aged specimens

shows that the normalized data converge almost entirely over each other. The absolute stress level versus cycles to failure as depicted in Figure 4.3 shows an

interesting trend. The trendlines are merely separated the respective static strengths for the various preconditions. Fatigue frequency effect depicted on Figure 4.4 shows a slight increased in damage at 2 Hz than at 10Hz. This could be due to statistical variation in fatigue data or due to damage accumulation with increasing time spent at a given applied stress level. Figure 4.5 shows the comparative plot for two different simulated fluid temperatures. There seem to be no significant difference in the degradation of the glass fiber-reinforced composite under these conditions as evinced by the slope of the fits. Glass/vinyl ester data for various conditions namely: temperature, moisture type and frequency is shown with Mandell's data in Figure 4.6.

It is interesting to note that the slopes on this plot are between 10-11% UTS/decade, which is consistent with the results, obtained by Mandell et al. [9-13]. It is evident from these data that for the conditions investigated namely: dry (as-received), wet (pre-aged in water at 45°C) and salt (aged in 3.5 % salt water at 65°C), dry-in-salt, dry at 20 Hz, Mandell's postulate seems to hold. Mandell and co-workers investigated fatigue effect due to fiber orientation, fiber volume fraction, resin type, and glass fiber type in polymeric composites. Mandell et al. observed a similar trend in the fatigue slope for the aforementioned variables, concluding that *the failure mechanism can be attributed to a fiber-dominated process*. In other words glass fiber composite fatigue failure occurs as a result of the gradual deterioration of the load-bearing fibers and it independent of the aforementioned parameters, namely: fiber volume fraction, resin type, glass fiber type, and fiber orientation.

Subsequent work by Sims et al. [37-38] collaborated Mandell's findings. Sims et al. investigated the effect of preconditioning (boiled and unboiled), pre-induced mechanical damage and orientation of reinforced material on glass fiber fatigue. Sims

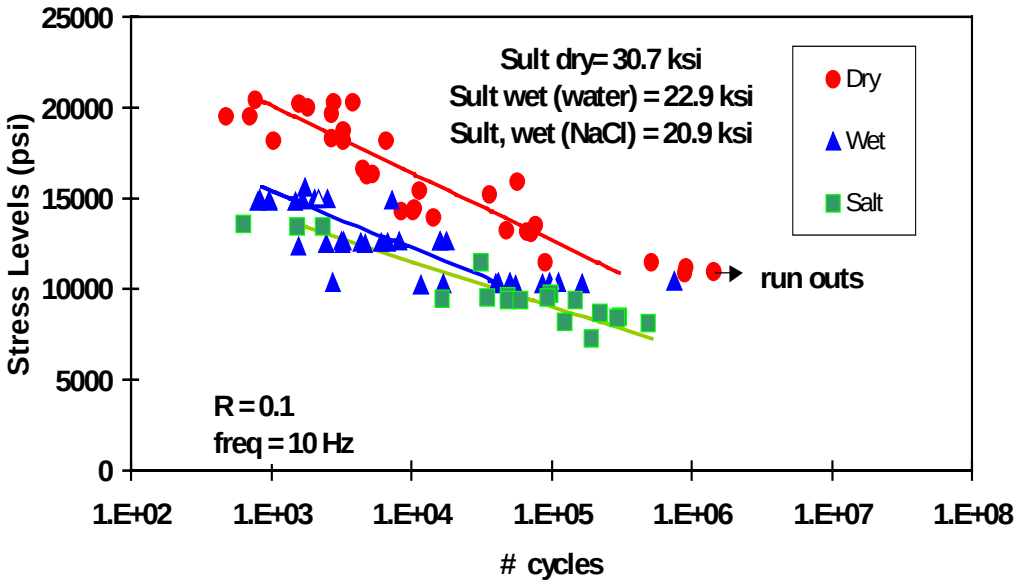

Figure 4.3: S-N curve in terms of absolute stresses

et al. concluded that, *independent of pre-conditioning treatment, orientation of reinforcement or preloading-induced mechanical damage, Mandell's stipulation lays credence to the concept of monotonic fatigue failure mechanism for glass fiber-reinforced composites.* These results validate Mandell's postulate that fiber-dominated mechanism is responsible for final composite failure, and further extend Mandell's variables to include: preconditioning, preloading and fiber architecture. One could also infer that the effect of temperature is implicit in the preconditioning aspect of Sims affirmation.

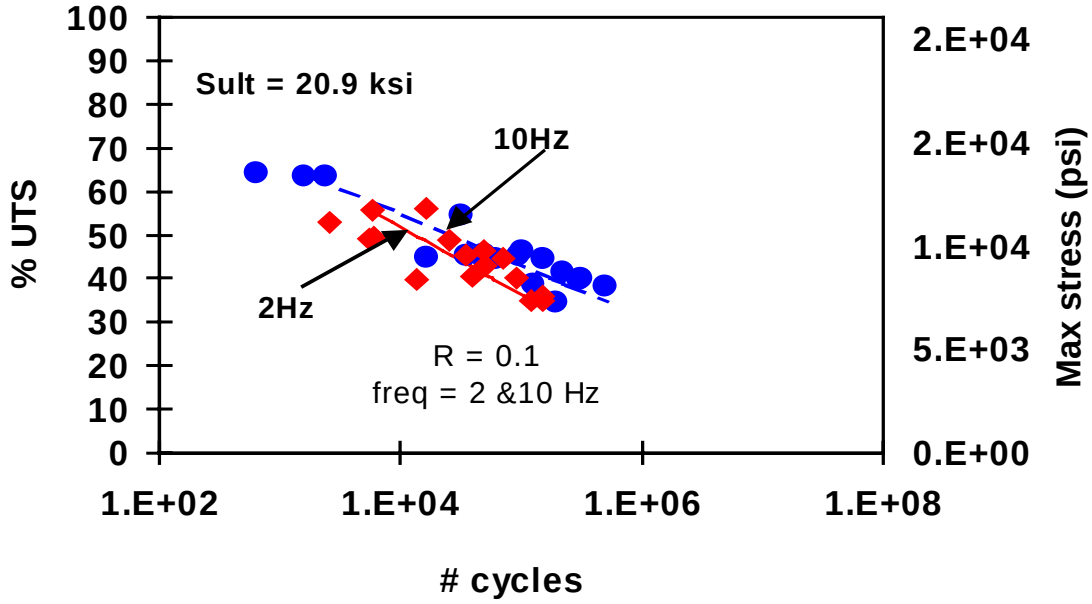

Figure 4.5: S-N at 2 & 10 Hz, 35°C

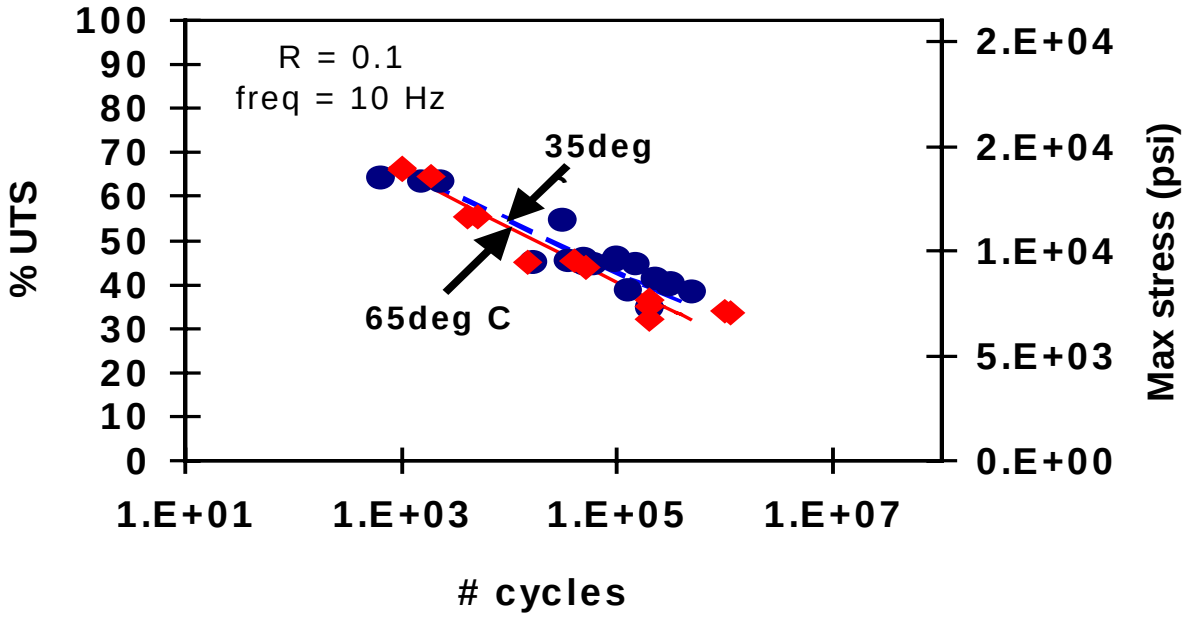

Figure 4.4: S-N curves at 30 & 65°C

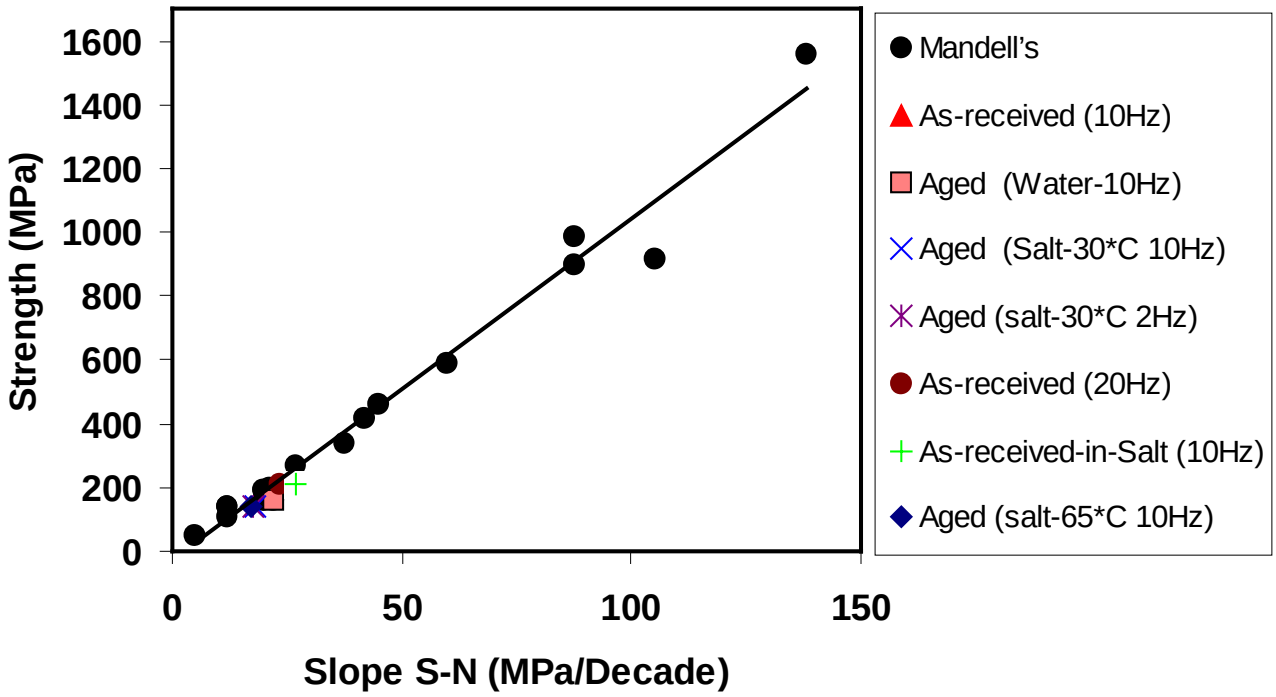

Figure 4.6: Mandell's relationship between tensile strength and the slope S/Log N curve, B for different materials. Values are included for EXTREN™- for various frequencies and testing conditions.

4.3 Residual Strength

Residual strengths of specimens tested to preset cycles were evaluated quasi-statically. The residual strength data were fitted to the Broutman-Sahu equation of the form in 4.4 with an $\alpha = 1$ [54]. Residual at 2 and 10 Hz is shown in Figure 4.7.

$$\frac{\sigma_{res}}{\sigma_{ult}} = 1 - \left(1 - \frac{\sigma_a}{\sigma_{ult}}\right)\left(\frac{n}{N}\right)^{\alpha} \qquad (4.4)$$

where:

σ_{res} = residual strength

σ_{ult}= ultimate tensile strength

σ_a = stress level

n = number of cycles

N = average life

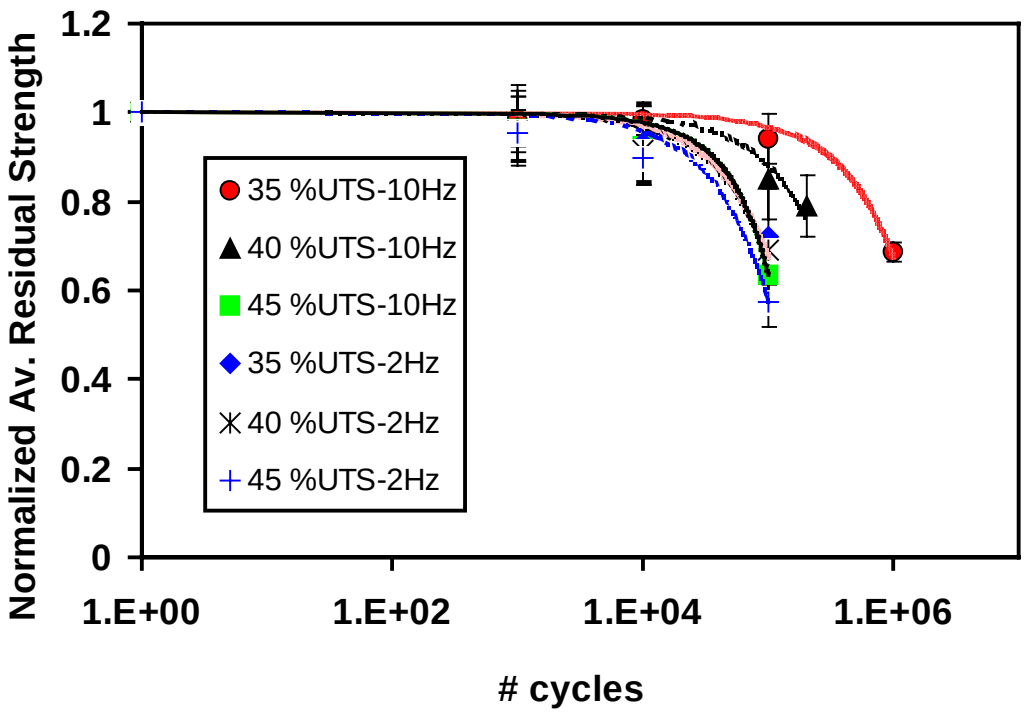

Figure 4.7: Normalized residual strength

Three load levels were evaluated at each frequency. There was progressive damage with increasing percent UTS as shown in the Figure 4.7. The cumulative plot of the residual strengths depicted in Figure 4.7 indicate slightly more damage occurring at 2 Hz than at 10 Hz. There is also progressive drop in strength with increasing applied stress levels at both frequencies. The standard deviation bars for both frequencies overlap considerably, indicating that differences in damage are not exceedingly different, but may suggest the presence time-dependent degradation characterization. Thus, the degradation of the material is observed from the residual strength plots to be more prominent at 2 Hz than at 10Hz.

4.4 Residual Modulus

The residual modulus characterizes changes in the material stiffness when subjected to preset cyclic loading and then quasi-statically tested. Reduction in modulus was slightly prominent at 2Hz as observed during testing.

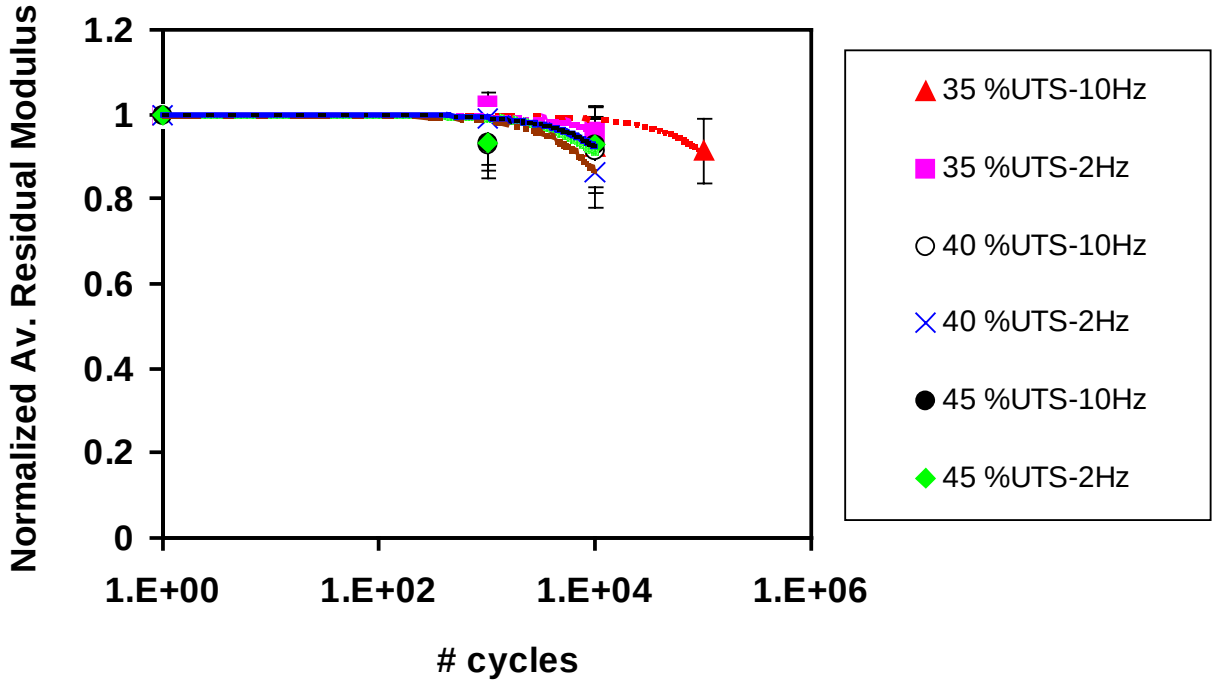

Figure 4.8: Normalized residual modulus

A fit for the residual modulus at 2 and10 Hz respectively, is shown in Figure 4.8. It can be inferred from Figure 4.8 that damage progressed with increasing load levels, but the overlapping of the standard deviation bars indicate that changes in modulus with frequency is insignificant except for the obvious fact that at 2 Hz specimen life dropped considerably, i.e. no data was obtained beyond 10^4 cycles at 2Hz. This slight difference in frequency effect could be attributed to the expended time a specimen is subjected to at the different frequencies, that is more time is spent at 2 Hz than at 10 Hz for the same applied stress level.

4.5 Residual Poisson's Ratio

The Poisson's ratio was obtained as a post-fatigue parameter of the glass vinyl ester system. This was obtained at 2 and 10Hz respectively. A normalized plot is shown in Figures 4.9. There seem to be no significant changes in the residual Poisson's ratio at the different preset cycles. The distribution in the data is fairly even.

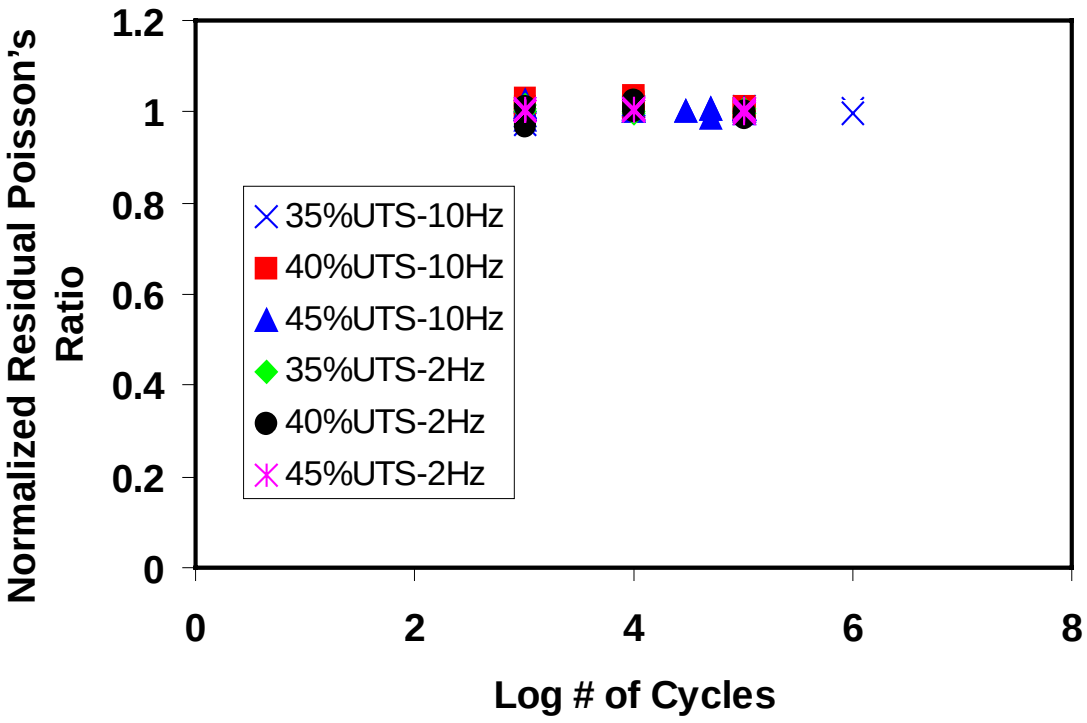

Figure 4.9: Normalized residual Poisson's ratio

The evenness of the distribution on the Poisson's Ratio data can potentially be attributed to the CSM in the composite. The CSM in the crosswise direction contains

proportionately more zeros and therefore can resist changes in Poisson's Ratio than in the transverse direction.

Chapter 5 : MODELING AND SIMULATION

5.1 MODELING AND SIMULATION: Motivation

Work by Mandell et al. [1,2] led to the conclusion that independent of fiber orientation, fiber volume fraction, resin type and fiber type, fatigue damage in polymeric composites is a fiber-dominated mechanism. Consequently, failure occurs as a result of the gradual deterioration of the load-bearing fibers. A wide range of experimentation using different resin systems, fiber types (continuous and discontinuous) and various fiber orientations, except that with stitched and woven architectures, backed this postulate. Figure 4-6 depicts Mandell's experimental work showing data points for a variety of fiber architectures, resin type and fiber type as well as a variety of orientations of reinforcement material. Mandell et al. realized that for a wide and different glass-fiber reinforced plastics the ratio of σ_f/B from equation 2.6, is a constant of value 10 %UTS/decade. Mandell's work has been substantiated by Sims and Gladman [5, 6], McBagonluri et al. [55-57] and to a large extend by Jones and co-workers [39].

It is evident from the foregoing analysis that there exist a fiber-dominated mechanism responsible for the failure of polymeric composites, and its dominance is also independent of moisture content as evinced by the EXTREN™ data in Figure 4.2-4.3.

Mandell's work raises a couple of issues that must be addressed if a viable and reliable life prediction model is to be development for the characterization of the durability and damage tolerance of glass-reinforced composites, especially in the infrastructure sector where longevity (50-75 years) is essential. Some of the issues that need immediate attention are:

1. What is the nature of the failure mechanism in the fatigue of glass fiber-reinforced composites?
2. Is the mechanism similar in both dry and moist environments?
3. Is the mechanism affected by fatigue frequency?
4. How could the knowledge of the failure mechanism help in the development of a micromechanics-based life prediction model(s) for creep and fatigue behavior of high performance polymeric composites?

Mandell's work provides answers to the first question. Work by McBagonluri et al., depicted in Figures 4.3-4.6, indicate that the fatigue failure of glass-fiber reinforced plastics is independent of moisture exposure. That is, the slope of the applied stress versus number of cycles curve indicate similar fractional drop in tensile strength per decade cycles, and it is independent of preconditioning in moist environment. Thus, the second and third questions have been addressed by the aforementioned experimental work. Fatigue frequency effect and a life prediction micromechanics-based approach for creep and fatigue behavior is the focal point of this thesis.

5.2 Synthesis of Simulation Model

This chapter, which uses Mandell's stipulation as guidance for the fatigue failure of fiber-reinforced composites, will coalesce a fracture mechanics-based residual strength model and the numerical lattice Green's function model developed by Curtin et al. [8], for the simulation of creep rupture and fatigue behavior of fiber-reinforced composite systems.

5.2.1 Curtin's Green Function Lattice Model

The lattice Green's function model is a numerical model for investigating the failure of reinforced composites. It makes use of 3-D Lattice Green's Function to compute load transfer from broken to unbroken fibers by also including the effect the fiber/matrix sliding. By incorporating a spatial parameter the nature of the load transfer can be altered for the local load sharing and the global load sharing case respectively [8,58].

The principal assumptions underlying the Lattice Green Function Model are as follows:

- Tensile failure in FRP is dominated by fiber bundle failure
- Elasticity theory is applicable in matrix transfer of load
- Load carried by matrix is zero after matrix cracking

- Stress along a fiber depend on applied stress and traction

Curtin's model simulates the failure strength of a unidirectional composite as depicted in Figure 5-1 below. The simulation process involves the discretization of the composites as shown in Figure 5-2.

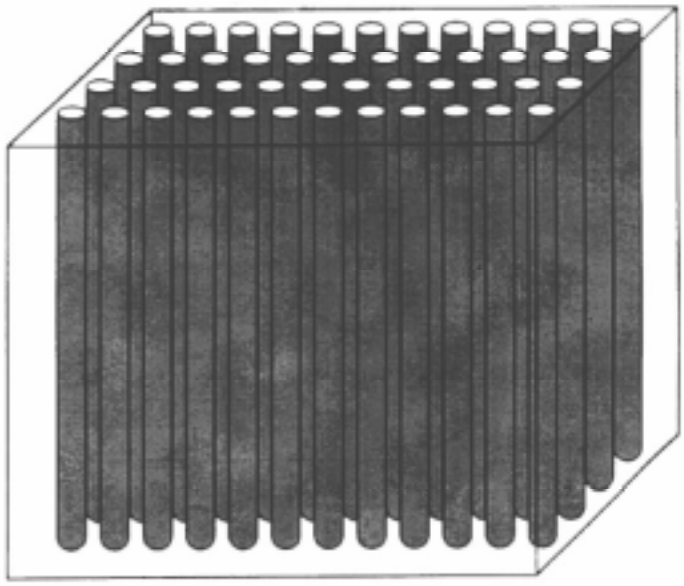

Figure 5.1: Unidirectional Fiber-Reinforced Composite (58)

5.2.2 Synthesis of Residual Strength Model for Glass Fiber Fatigue

The residual strength model concentrates on the development of a crack propagation model describing the fiber-dominated fatigue postulate proposed by Mandell et al. This model stipulates that the accumulation of damage in the fiber is accounted for in the crack growth that occurs as a result of the fractional time spent at

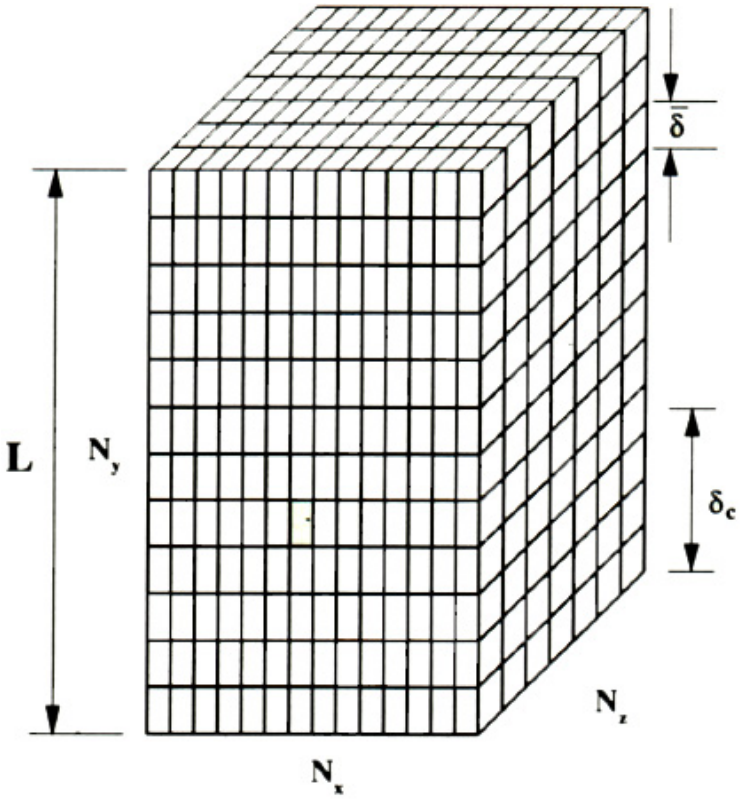

Figure 5.2: Partitioning of the simulated composite showing the length scale (ref. 58)

a damaging stress level. Thus, in its entirety the residual strength model characterizes glass fiber failure from a crack propagation perspective. This model is similar to

Ritter's [15]. The divergence in the derivations occurs in the assumptions. While Ritter discards the stress intensity parameter, this is simply absorbed into the constant term C in the current model. Also the current model does not incorporate the inert strength, but instead approximates it with the ultimate tensile strength.

The residual strength model begins with the power law description of crack growth velocity in a glass fiber.

$$\frac{da}{dt} = AK_I^N \tag{5.1}$$

where K_I is given by Eq. 5.2a, and the critical stress intensity factor is defined as in 5.2b.

$$K_I = \sigma Y\sqrt{\pi a}$$
$$K_{IC} = \sigma_r Y\sqrt{\pi a} \tag{5.2a\&b}$$

where:

σ = applied stress

a = flaw size, a

σ_r = residual strength

we obtain 5.3 by substituting 5.2 into 5.1

$$\frac{da}{dt} = A\left[\sigma Y\sqrt{\pi a_o}\right]^N \tag{5.3}$$

by integrating equation 5.3 from an initial flaw size, a_o to a final flaw size a, we obtained

$$\int_{a_o}^{a} a^{-\frac{N}{2}} da = AY^N \pi^{\frac{N}{2}} \int_0^{t_f} \sigma(t)^N dt \tag{5.4}$$

simplifying Eq. 5.4 further we obtain

$$\left(\frac{a}{a_o}\right)^{1-\frac{N}{2}} = 1 + \frac{\left((1-\frac{N}{2})AY^N \pi^{\frac{N}{2}}\right)}{a_o^{1-\frac{N}{2}}} \int_0^{t_f} \sigma(t)^N dt \tag{5.5}$$

where σ (t) is the local fiber stress at time, t.

5.2.2.1 Failure Criteria

Using the failure criterion that at a given crack length failure occurs when equation 5.6 is true and assuming that initial ultimate strength is controlled by brittle fracture, we can relate the critical intensity factor to the fracture toughness of the fiber as in 5.6

$$K_I = K_{IC}(a_o, \sigma_{ult}) = \sigma_{ult} Y \sqrt{\pi a_o} \tag{5.6}$$

Thus, at a given time, t the remaining strength of the fiber is simply the stress required for K_{IC} to be equal K_I at the current flaw size, a.

We can divide equation 5.2a by 5.2b to obtain

$$\frac{\sigma_r}{\sigma_{ult}} = \sqrt{\frac{a_o}{a}} \tag{5.7}$$

Substituting equation 5.7 into equation 5.5 we obtain equation

$$\frac{\sigma_r(t)}{\sigma_{ult}} = \left\{ \frac{1-\left(\frac{N}{2}-1\right)AY^N \pi^{\frac{N}{2}} \sigma_{ult}^N}{a_o^{1-\frac{N}{2}}} \int_0^t \left\{ \frac{\sigma(t)}{\sigma_{ult}} \right\}^N dt \right\}^{\frac{N}{2}} \tag{5.8}$$

equation 5.8 simplifies to

$$\frac{\sigma_r(t)}{\sigma_{ult}} = \left\{ 1 - C\int_0^t \left\{ \frac{\sigma(t)}{\sigma_{ult}} \right\}^N dt \right\}^{\frac{2}{N-2}} \tag{5.9}$$

where C is given by

$$C = \frac{1-\left(\frac{N}{2}-1\right)AY^N \pi^{\frac{N}{2}} \sigma_{ult}^N}{\pi^{\frac{N-2}{2}} K_{IC}^{2-N} \sigma_{ult}^{N-2} Y^{N-2}} \tag{5.10}$$

By employing stress rupture data we can obtain the parameters N and C.

5.2.2.2 Case I: Creep Rupture Case

In the static case a constant stress is applied and incremented while the composite breaks are monitored. The time-dependent stress in equation 5.9 is replaced by a constant stress as in 5.11. Equation 5.12 is a consequence of a substitution with equation 5.11.

$$\sigma(t) = \sigma_a = const \tag{5.11}$$

$$\left(\frac{\sigma_a}{\sigma_{ult}}\right)=\left[1-C\left(\frac{\sigma_a}{\sigma_{ult}}\right)^N t_r\right]^{\frac{1}{N-2}} \tag{5.12}$$

By solving equation 5.12 for t_r we can obtained the time to failure of the composite.

$$t_r=\frac{-\left(\frac{\sigma_a}{\sigma_{ult}}\right)^{N-2}+1}{C\left(\frac{\sigma_a}{\sigma_{ult}}\right)^N} \tag{5.13}$$

Simplifying further we obtain

$$t_r=\frac{1}{C}\left\{1-\left(\frac{\sigma_a}{\sigma_{ult}}\right)^{N-2}\right\}\left(\frac{\sigma_a}{\sigma_{ult}}\right)^{-N} \tag{5.14}$$

5.2.2.3 Case II: Fatigue

In the fatigue case, a sinusoidal wave function

$$\sigma(t)=\Psi+\Phi\sin(2\pi ft) \tag{5.15}$$

Where ψ and Φ are maximum and minimum stress relations and are defined as follows:

$$\sigma_{\min}=R\sigma_{\max} \tag{5.16}$$

$$\Phi=\frac{\sigma_{\max}-\sigma_{\min}}{2} \tag{5.17}$$

$$\Psi = \frac{\sigma_{\max} + \sigma_{\min}}{2} \tag{5.18}$$

By substituting equations 5.16-5.18 into equation 5.15 and simplifying further we obtain equation 5.19.

$$\sigma(t) = \frac{\sigma_{\max}}{2}\left[(1+R)+(1-R)Sin(2\pi ft)\right] \tag{5.19}$$

Where:

σ_{max} = maximum %UTS

R = stress ratio

f = frequency

t = time

By integrating equation 5.19 from an initial period 0 to a given period 1/f, and substituting the results into equation 5.14 we obtain the residual strength of a single fiber any given time, t.

5.3 Simulation Procedure

Figure 5.4 shows the detailed programming procedure for the simulation process. Using this model the failure of a composite of predetermined physical size can monitored. This is achieved by monitoring the remaining strength of the surviving fibers, the traction and stress distribution, and composite failure per a given load level. In its entirety, this model predicts the creep rupture and fatigue behavior of high

performance polymeric composites. The simulation process involves the discretization of the fiber bundle as shown in Figure 5.2, and the assignment of Weibull random distributed strengths to the discretized fiber elements. An applied stress is imposed on the composite and incremented until a specified stress level is attained where the dependency begins. The various stress levels are assigned based on the requirements of a given simulation session. Stresses in failed fibers are re-assigned to adjacent fibers. The redistributed stresses are much effective within the neighborhood of the break for the load sharing case and are sparsely so in the case of global load sharing. The shielding effects of innermost fibers reduce the stresses on distant fibers.

The redistribution of stresses can be evaluated in two ways, namely via Local Load Sharing (LLS) or Global Load Sharing by adjusting the spatial parameter. In the case of the Local Load Sharing, the shed load is confined to a defined region so as to induce a local stress concentration. In the case of Global Load Sharing, stresses are distributed equally along the span of the composite such that fibers within the same slip plane are exposed to the same incremented load and the global force equilibrium.

The model assumes that at the point of fiber failure, debonding occurs at the fiber/matrix interface. The sliding interfacial shear stress is assumed to be constant as depicted in Figure 5.3. Thus by balancing the shear load to the tensile load we obtain equation 5.2. Thus, at the point of fiber failure the stress is zero, but stress recovery occurs linearly to a far-field stress, σ_f at a slip length, l_s given by equation 5.3.

$$\frac{d\sigma_z}{dz} = \frac{2\tau}{r} \tag{5.2}$$

where:

r = fiber radius

σ_f = stress on fiber

τ = interfacial shear stress

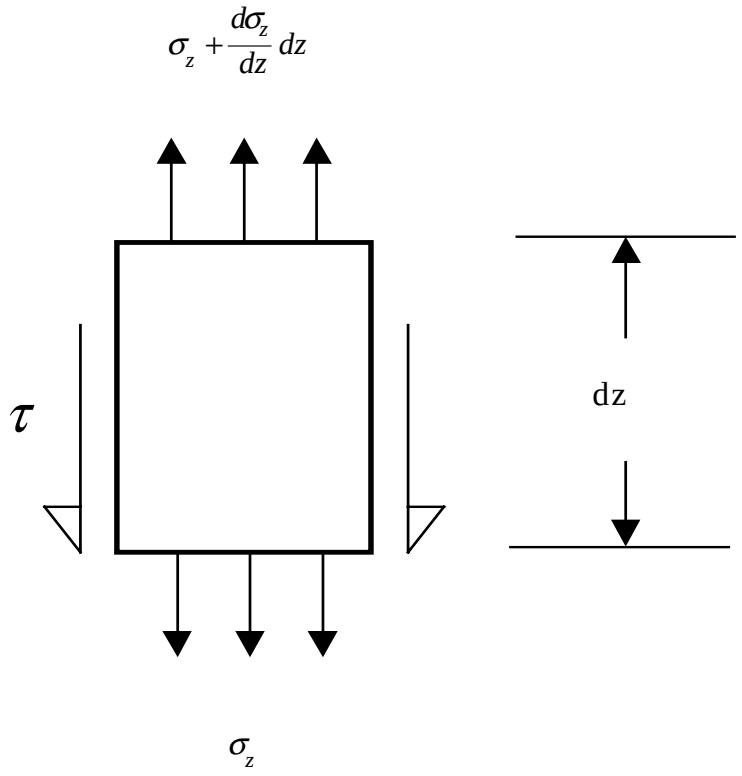

Figure 5.3: Fiber Debonding and Slip in a Fiber Element

$$l_s = \frac{r\sigma_f}{2\tau} \tag{5.3}$$

The discretized time-to-failure is computed for each discretized fiber and the minimum time is assessed. The fiber with the minimum incremented time-to-failure distributed time is broken, and the process is re-evaluated until complete failure of the composite occurs [58,64]. By replacing the constant stress with a sinusoidal wave function the procedure is modified for fatigue life prediction.

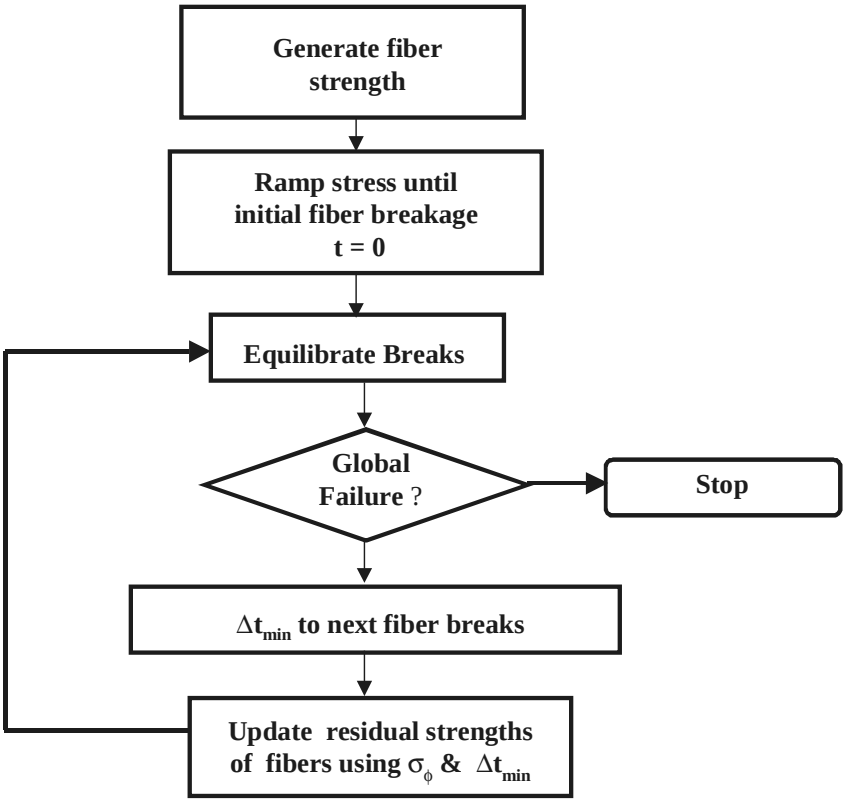

Figure 5.4: Flow Chart of Programming Procedure

5.3.1 Fiber Failure Criteria

Fiber failure occurs when the applied stress plus the transferred stress exceed the local residual strength. Conversely, mechanical equilibrium is maintained when the local stress is less the local fiber strength.

5.3.2 Composite Failure Criteria

Composite failure occurs as a result of a complete fiber breakage in a slip-length within a cross-sectional slip plane. In the static case composite failure occurs at a critical applied stress while in the rupture case, composite failure occurs at critical time at a critical applied stress.

5.4 Model Validation: Glass Fiber Data

The model requires fiber creep rupture data. This data is fitted to equation 5.1 to obtain the N and C parameters which are the corrosion susceptibility constant and the parameter C which is a constant embodying material properties of the fiber. Figure 5.5 shows a fit of equation 5.14 using fused silica creep data [59] and Table 5.1 shows the corresponding fit parameters for fused silica and E-glass fiber in 100% relative humidity [65]. In addition, the numerical LSS simulation model requires the Weibull strength parameters (σ_o, α at a given L_o), the interfacial sliding shear stress, τ the fiber radius, r which are used to compute the normalizing parameters σ_c and δ_c and the discretizing parameter, mc. Table 5.2 shows these inputs and the various sources.

Table 5.1: Fiber Fit Parameters For Creep Simulation

	PARAMETERS	
Fiber Type	N	C
E-glass	18.0	0.1
Fused Silica	20.0	0.1

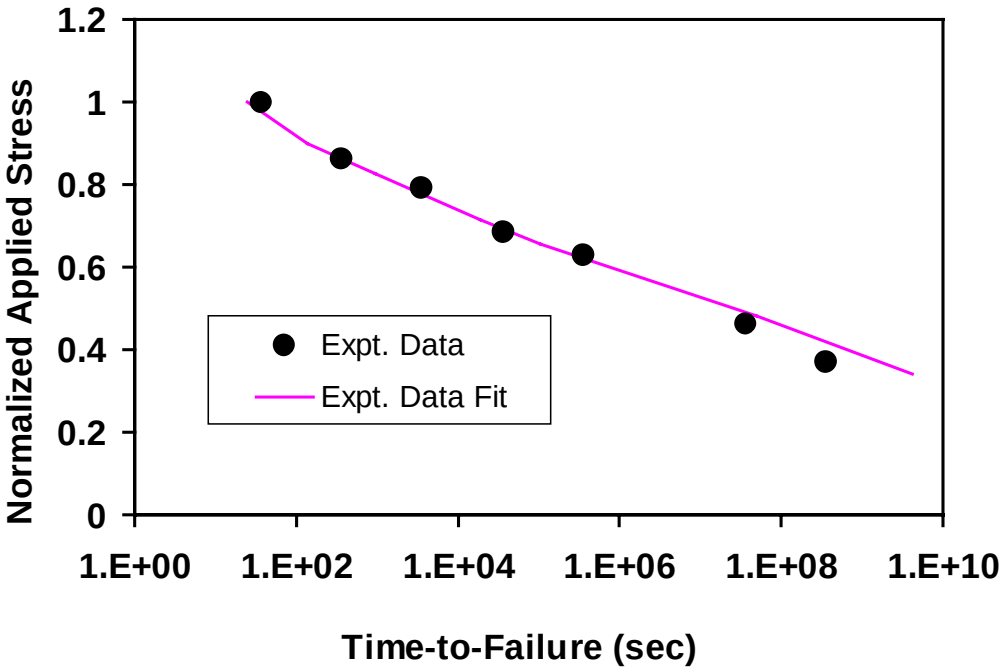

Figure 5.5: Fused Silica Data (59)

There was no fiber data for fatigue in the reviewed literature, therefore the N and C

values obtained from the fused silica and E-glass fiber creep data was used in the fatigue case as well.

Table 5.2: Shows Fiber Properties as inputs for the simulation model.

Parameter	Value	Reference:
α	7.6	60
β	14 MPa	58
σ_o	2520 MPa	60
τ	39 MPa	67
L_o	1 cm	60

5.4.1 Parametric Analysis

5.4.1.1 Composites Size and Tensile Strength

The fiber bundle strength is a function of composite physical size (length and number of fibers) and the initial Weibull strength distribution in the discretized fiber elements [3]. The relationship between composite size and tensile strength

$$\sigma_c = \left(\frac{\sigma_o^m \tau L_o}{r} \right)^{\frac{1}{m+1}} \tag{5.3}$$

$$\delta_c = \left(\frac{\sigma_o r L_o^{\frac{1}{m}}}{\tau} \right)^{\frac{m}{m+1}} \qquad (5.4)$$

Where:

L_o = gauge length

σ_o = gauge stress

m = Weibull modulus

τ = interfacial shear stress

r = fiber radius

σ_c, δ_c = characteristic strength and length respectively.

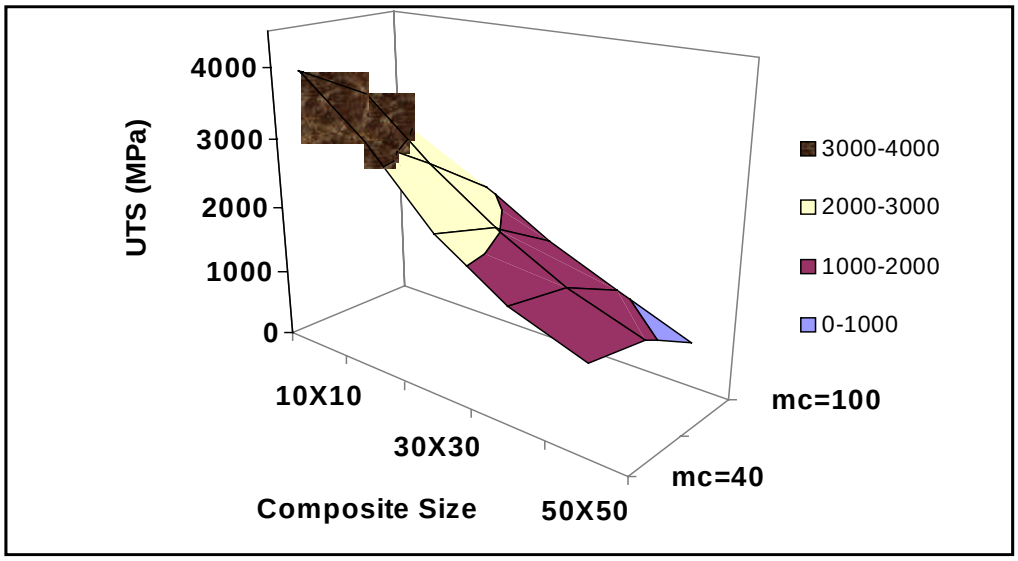

Figure 5.6: Tensile Strength and Composite Size for Fused Silica/Epoxy System

has been evaluated for the model. Figure 5.6 indicates a decrease in strength with increasing composite size. The parameter, mc embodies implicitly the composite length. Thus, by increasing fiber bundle size and length there is a higher probability of including defective fibers hence increased statistical distribution of flaws, leading to lower bundle strength and consequently, lower tensile strength. Thus, the fiber strength appears to be inversely proportional to the composite length [60].

The characteristic strength and length from the global load sharing (GLS) model are essential parameters for the normalization of the specific bundle strength to obtain the ultimate tensile strength of the composite. Equations 5.3 and 5.4 show the relationship between the characteristic parameters. The ultimate tensile strength of the fused silica/epoxy system was computed using equation 5.5. Foster [58] has shown that the tensile strength of Ti-1100 and Ti-6Al-4V metal matrix composites using the LLS simulation were consistent with experimental data to within 10% variation. For cases indicated in Figure 5.6 namely, mc=40, 60, 100 no convergence in tensile strength values was observed.

$$\sigma_{ult} = \nu\sigma_f + (1-\nu)\sigma_m \tag{5.5}$$

where:

σ_{ult} = ultimate tensile strength

σ_f = fiber bundle strength

σ_m = matrix yield strength

ν = Fiber volume fraction

5.4.1.1a Scaling Effects

Tables 5.3 and 5.4 show the strength distributions with length and volume respectively. In the case of implicit lengths against Weibull strengths the Weibull modulus obtained was about 1.9 while in the case of the composite volume against strength the Weibull modulus was 2.8. The discrepancy in the Weibull moduli for the length and volume analysis is not known at the moment, but by increasing the number of simulations per a load level as well as increasing composite size the discrepancies in scaling effects may be rectified.

Table 5-3: Two-Parameter Weibull Strengths at three implicit lengths

Implicit Length	Weibull Strength
40	2877
60	2505
100	1782

Table 5-4: Composite Volume with corresponding Composite Strength

Composite Volume	Composite Strength
100	4030
400	3270
900	229
1600	1630
2500	1280

5.4.1.2 Fatigue Frequency Effects

The effect of fatigue frequency on the degradation of composite systems has been a source of contention in the composite community. Chapter 3 discusses the issue in detail referring to the various schools of thought. As indicated in Figure 5.7 there was no significant drop in fatigue performance with increasing frequency. Figure 5.7 indicates that frequency is nearly invariant in the fatigue simulation model.

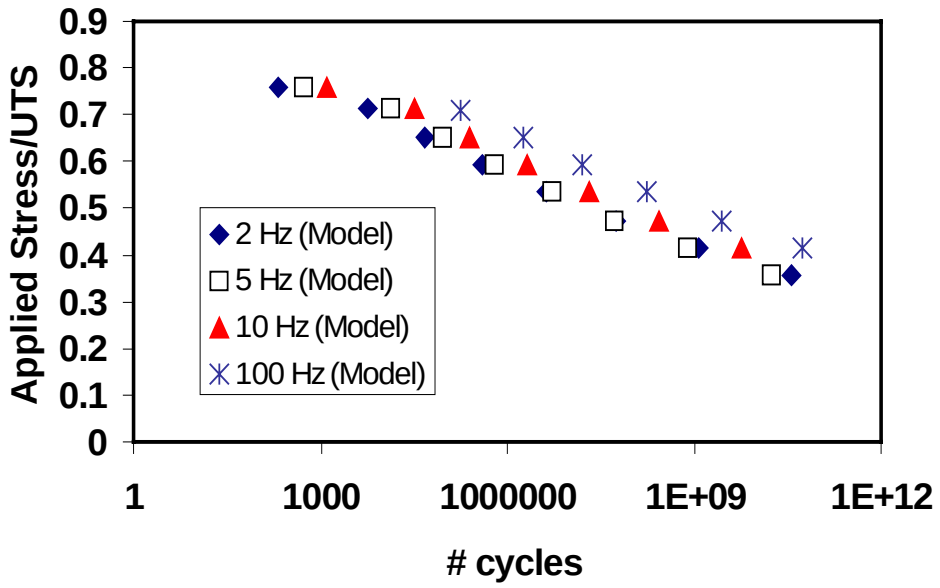

Figure 5.7: Fatigue Frequency Effect

5.4.1.3 Composites Failure: Creep and Fatigue

This simulation models creep rupture failure of composite at various prescribed normalized stress levels is as shown in Figure 5.8. Each stress level indicates an average of fifty composite failures. The corresponding probability distribution of failure times is shown on Figure 5.8 with its corresponding Weibull parameters.

Frequency distribution is shown in Figure 5.10. The distribution is skew to the left with Weibull parameters as shown in Figure 5.9. Figure 5.9 represent about 100

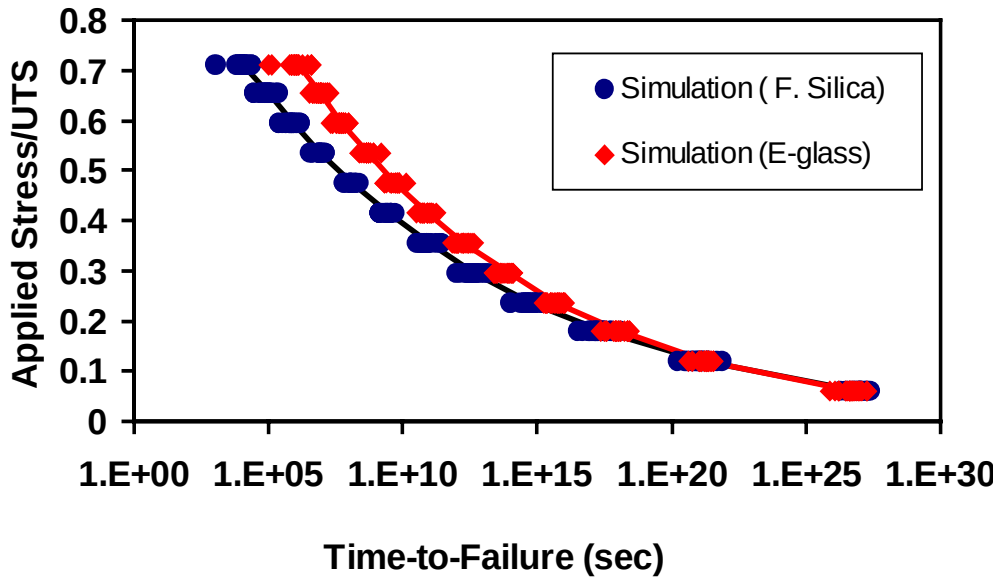

Figure 5.8: Composite Creep Rupture Simulation

simulation of creep rupture failure at a single applied stress level. Thus, when subjected to the same stress levels composite failures exhibit dispersion as will be

expected in the laboratory environment.

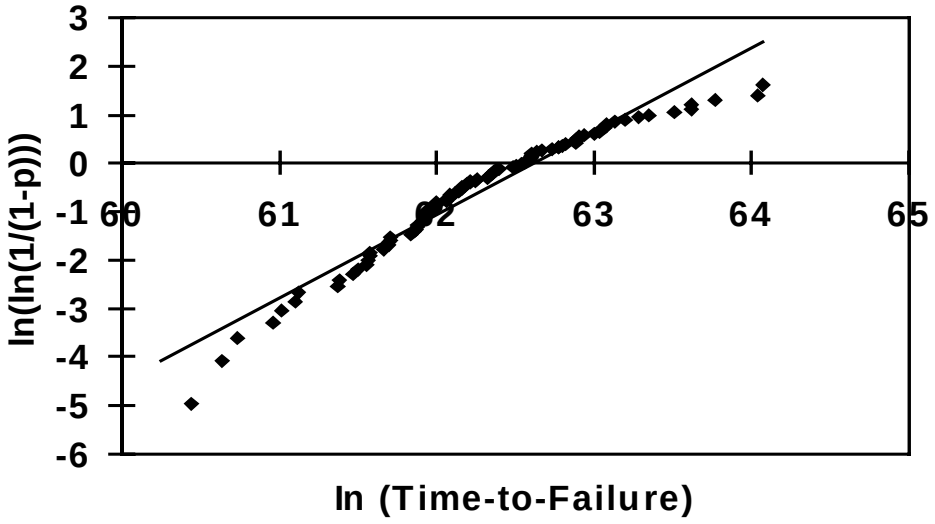

Figure 5.9: Weibull Distribution of Creep Failure Times

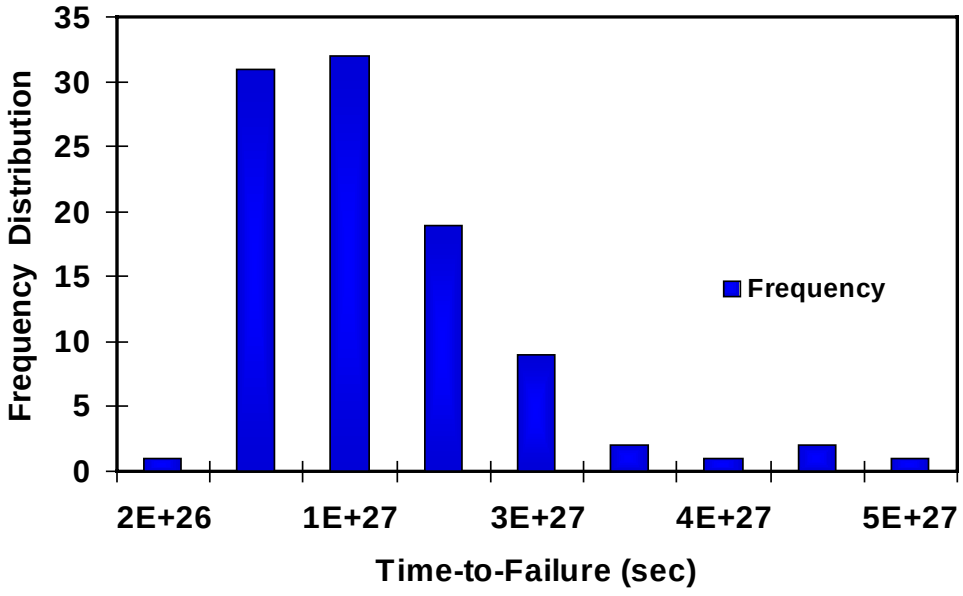

Figure 5.10: Frequency Distribution of Failure Times at a given stress level

Composite Fatigue failure distribution for various load levels is indicated in Figure 5.11. Also shown in Fig. 5.11 is the average failure at a given load level. Composite life decreases with increasing load levels as will be expected.

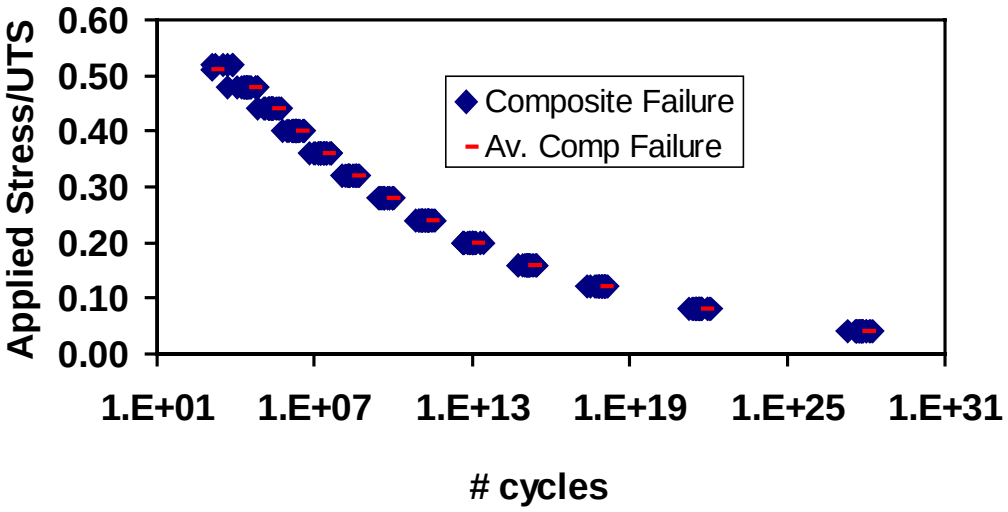

Figure 5.11: Composite Failure Distribution at different Load Levels

5.5 Comparison of Model with Experimental Data

5.5.1 Creep Rupture

Creep simulations for glass-epoxy systems are shown in Figures 5.12 and 5.13. In the absence of S-2 glass creep data in the reviewed literature, the model was validated using fused silica creep data. Fused silica has a theoretical strength between 10-20 GPa, and a thermal conductivity close to that of S-2 glass as indicated in Table

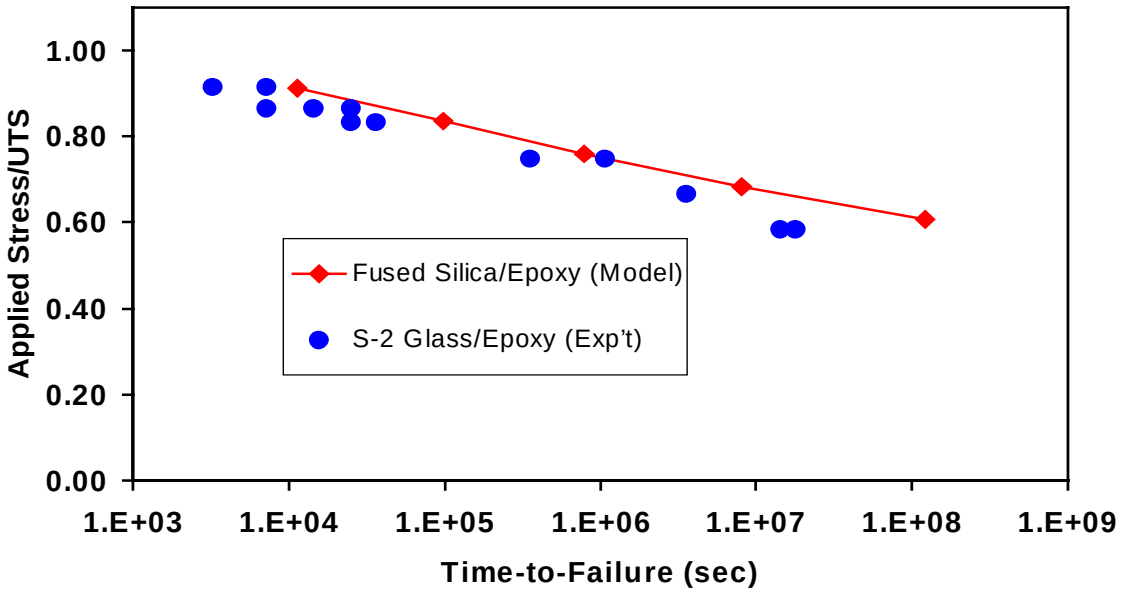

Figure 5.12: Creep simulation of S-2 Glass/Epoxy (61)

5.5. The creep data for S-2 glass/epoxy, in calcium hydroxide of pH13, compares quite well with data obtained from the simulation, using fused silica inputs as indicated in Table 5.1. The S-2 glass/epoxy data was normalized by the initial tensile strength of 2070MPa and for the simulated data, the applied stress was normalized by the tensile strength of the physical composite size (30X30). Figure 5.13 shows the creep rupture

plots for E-glass/epoxy system and the corresponding simulated model using E-glass properties indicated in Table 5.1. In spite of the scatter in the experimental data, the simulated model seems to represent a realistic representation of creep rupture behavior for the given S-2/epoxy system. The slopes of these curves are about 14-15 %UTS/decade.

Table 5.5: Glass Fiber Properties

Fiber	Strength (GPa)	Modulus (GPa)	Thermal conductivity (W/m.°K)	Reference
S-2 glass	4.9 (23°C)	86.9 (23°C)	1.45	61
Fused silica	10-20	72 (Room Temp)	1.4	61, 62, 63
E-glass	3.4 (23°C)	72.3 (23°C)	1.3	61

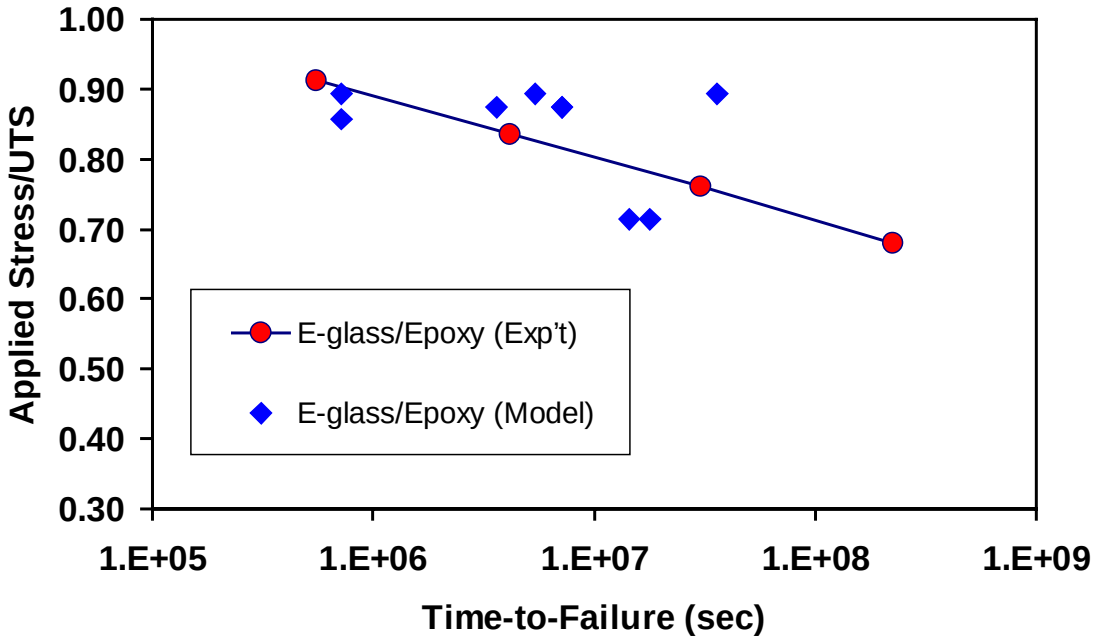

Figure 5.13: Creep Simulation of E-Glass/Epoxy (61)

5.5.2 Fatigue Performance

Fatigue simulation from the model is shown in Figure 5.14 with experimental data for unidirectional fiber-reinforced composite [38]. Simulations were run at 2, 5, and 10Hz. It is evident from Figure 5.14 that the simulated data progressively mimic a realistic trendline fit for the experimental data, especially that of the UCFR. The rate of strength per decade for the UCFR and the UCMFR are 10.2 and 13 respectively. It is interesting to note that the slope for the simulated fatigue data is between 12-14 UTS/decade.

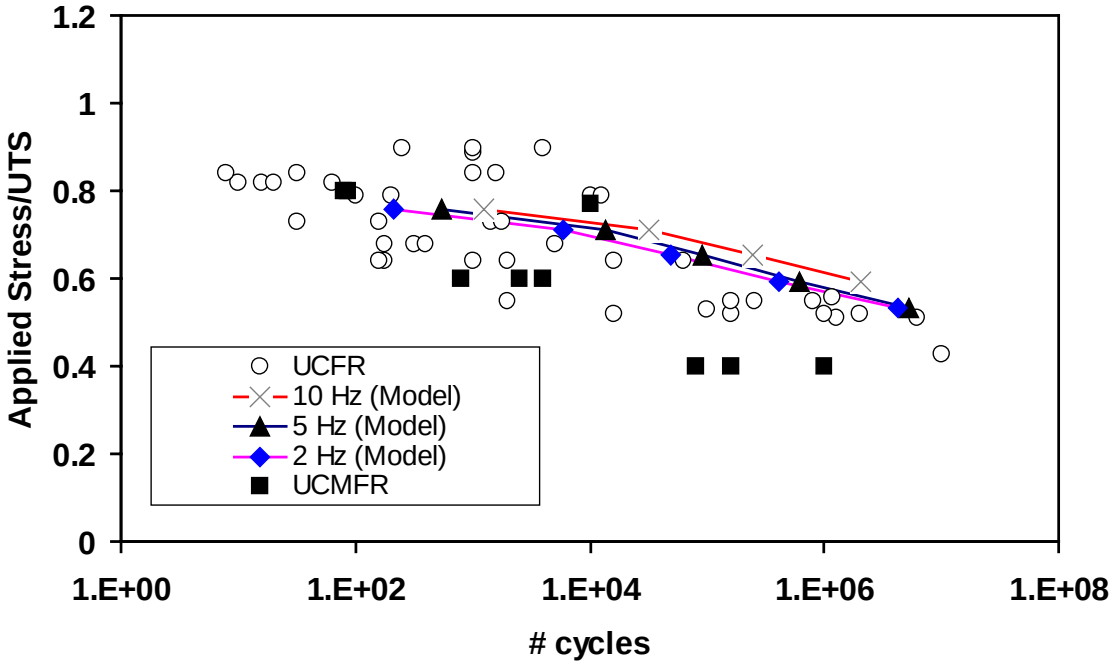

Figure 5.14: Fatigue Simulation of E-Glass/Epoxy

Chapter 6 : SUMMARY, CONCLUSION & RECOMMENDATIONS

6.1 Summary

This thesis has presented the experimental evidence substantiating Mandell's assertion that a fiber-dominated damage mechanism is the driving force behind the failure of fiber-reinforced polymeric composites. Using Mandell's postulated as a premise, a micromechanics-based life prediction simulation model was developed, by assimilating the Lattice Green's Function Numerical approach proposed by Curtin et al. and a fracture mechanics-based residual strength model. The LLS model was ideal for the modeling processes since the principal assumption that *fiber failure controls composite failure is a corollary of Mandell's postulate.* The fatigue and creep rupture models developed are comparable to existing experimental data.

6.2 Conclusion

Thus, by combining the statistical- and numerical LLS models with the fracture mechanics-based residual strength model, we developed a model to characterize the creep rupture and fatigue performance of polymeric composites. Results obtained from the creep and fatigue models compared well with available experimental data. Mandell's postulation that the fatigue curves for polymeric composites have slope of about 10 %UTS/decade compares well with the results obtained from the simulation model. There is however, ample evidence in the literature [9,40] and the present model, to substantiate that the 10 %UTS/decade is a *conservative estimate* for the rate

of strength lost per a decade. Mandell for instance obtains values slightly beyond 11 %UTS/decade, while Demers' data show up to about 14.5 % UTS/decade and C. J. Jones et al. [39] reported a 13.0 %UTS/decade. It will be proper if a coefficient of variation or a performance bounds is placed on the 10 %UTS/decade. There is no doubt however, that for glass fiber-reinforced composites the rate of decay of strength, B is within the range $10< B<20$.

6.3 Recommendations

The following are some of the essential sectors of life prediction methodologies that require further attention. The current model incorporates some of the salient features of a reliable life prediction procedure, such as the assignment of Weibull strength (statistical) to fibers, and the inclusion of a crack propagation model (Fracture mechanics). The following recommendation highlights the core attributes of a viable life prediction methodology and delineates the areas where further endeavors should be concentrated.

1. Damage-evolution of material properties as function of loading history must be assessed for a given application environment, this will foster the development of mechanistic models to characterize fracture damage and failure mechanisms in polymeric composites per an environment. Current life prediction methods take care of the local stress distribution not the material state after damage evolution.

2. Interaction between local stress distribution and/or stress concentration with matrix cracks, delaminations, fiber-matrix debonding, may affect residual strength computations. It is essential that a unified life predictive model recognize the interaction of failure modes and damage processes.

3. Fiber bundle strength may be altered by material degradation processes such as oxidation or other chemical or thermo-chemical processes, which require further substantiation.

4. Statistical properties of material systems as well as its performance distribution should be assessed for all potential simulated application environments so that life methodologies may incorporate a level of statistical confidence. This could lead to the evolvement of better methods for assessing material variability, and foster the development of comprehensive scholastic processes for composite characterization.

5. Life prediction methods incorporating the statistical interaction between damage mechanisms or failure modes will be essential in the analysis of representative volume elements and allow for the generality of life prediction methodologies.

6. The interaction between life prediction methods, reliability, manufacturing processes and general performance qualities will provide a more realistic and well-defined approach to life prediction for structural design.

7. NDE techniques should be used in conjunction with simulation models to characterize progressive damage during the fatigue failure of fiber bundles.

8. Graphical Visualization tools should be developed to enhance the visualization of the damage processes [66].

Chapter 7 : REFERENCES

[1] Ian Kummerow et al., “Design & Development of a Composites Marine superstructure for a Fast Catamaran Ferry,” *Proceedings of 7th International Conference on Marine Applications of Composites Materials* March 17-19, Melbourne, Fl 1998.

[2] R C Roberts, “The Effect of Chemical Environments on the Mechanical Properties of GRP,” *Symposium on Reinforced Plastics in Anti-Corrosion Application*, National Engineering Laboratory, East Kilbride 26-27 September 1979 Glasgow.

[3] Ronnal Reichard, “Composite Super Structure System for Ships,” *Proceedings of 7th International Conference on Marine Applications of Composites Materials,* March 17-19, Melbourne, Fl 1998.

[4] Sven-Erik Hellbratt et al., “Advanced Composites- The future Material in both Naval and Commercial Shipbuilding, Design & Development of a Composites Marine superstructure for a Fast Catamaran Ferry,” *Proceedings of 7th International Conference on Marine Applications of Composites Materials,* March 17-19, Melbourne, Fl 1998.

[5] F. J. Fischer & M. M. Salama, “Emerging and Potential Composites Applications for Deepwater Operations,” *Composites Engineering & Applications Center for Petroleum Exploration and Production U. of Houston,* Houston, TX.

[6] L. S. Norwood & B. R. Taylor, “Resins Systems for GRP Fuel Storage Tanks,” *BPF* November 1992.

[7] Michael D. Hayes, “Characterization and Modeling of a Fiber Reinforced Polymeric Composite Structural Beam and Bridge Structure for Use in the Tom’s Creek Bridge Rehabilitation Project,” *MS Thesis* Virginia Polytechnic Institute & State University Blacksburg,VA February 1998.

[8] S. J. Zhou & W. A. Curtin, “Failure of Fiber Composites: A Lattice Green Function Model,” *Acta metall. mater.* Vol 43, No. 8 pp 3093-3104, 1995

[9] J. F., Mandell, “Fatigue Behavior of Fibre-Resin Composites,” *in Developments in Reinforced Plastics* 2, Properties of Laminates ed. G. Pritchard 1978.

[10] J. F. Mandell, D. Huang & F. J. McGarry, Proc. 35th *Technical Conference on Reinforced Plastics/CI of SPI*, 1980 19-A

[11] J. F. Mandell, F.J. McGarry W. D. Barton & R. P. Demchik*, in Proc. 31st R. P. /C. Inst., Society of the Plastic Industry,* 1976, paper 21B.

[12] J. F. Mandell, *Polymer Composites,* 1981 2, 22.

[13] J. F. Mandell, D. Huang & F. J. McGarry, *Proc. 37th on Reinforced SPI /CI* 1982 paper 23C.

[14] S. M. Wiederhorn, *J. Am. Ceram*. Soc. 50 407, 1967.

[15] J. E. Ritter, “Probability of Fatigue Failure in Glass Fibers,” *Fiber & Integrated Optics, Vol 1 No 4. 1978.*

[16] J.E. Ritter, Jr. & C. L. Sherburne, *J. Am. Ceram. Soc.,* 54, 601, 1971.

[17] J.E. Ritter, Jr. & J. Manthurithil, *Glass Technology*, 14, 60, 1973.

[18] J.E. Ritter, “Strength and Fatigue of Silicate Glasses,” in Strength of Inorganic Ed. Charles R. Kurkjian, Plenum Press.

[19] P.K Mallick. Fiber Reinforced Composites. Dekker, 1988: New York, NY.

[20] O.P. Gillat and L.J. Broutman. “Moisture in Epoxy Resin Composites,” *J. Adhesion, 12: 153 (1981).*

[21] Adamson, J. Michael, “A Conceptual Model of the Thermal-Spike Mechanism in Graphite/Epoxy laminates,” *Long-Term Behavior of Composites, ASTM STP 813, T.K.O’Brien, Ed. ASTM, Philadelphia, 1983*.

[22] Hofer, K. E, G.N. Skaper & L.C. Bennett, & N. Rao, “Effect of moisture on fatigue & Residual strength losses for various composites,” *Journal of Reinforced Plastics & Composites* Vol 6 JAN 1987.

[23] M.D. Hayes, K. Garcia, N. Verghese, J. J. Lesko, “ The Effects of Moisture on the Fatigue Behavior of Glass/ Vinyl Ester Composite, *Fiber Composites in Infrastructure.*

Ed. H. Saadatimanesh, M. R. Ehsani, ICCI '98, Tucson, AR. 5-7 Jan. 1998.

[24] Shanker et al., "Hygrothermal Effects on Chopped Fiber/Woven fabric Reinforced Epoxy Composites Part A: Moisture Absorption Characteristics*" J. of Reinforced Plastic Composites*. V 10 n 5 Sept. 1991, p 446-456. Brookfield: 1996

[25] H. A. Barker, I. G. Baird-Smith & F. Jones, Large Diameter GRP pipes in Civil Eng.- The Influence of Corrosive Environments, *in Symposium on Reinforced Plastics in Anti-Corrosion Application,* National Engineering Laboratory, East Kilbride 26-27 September 1979 Glasgow.

[26] A.G. Metcalfe & G. K. Schmitz, "Mechanism of Stress Corrosion in E-glass Filaments," *Glass Technology Vol. 13 No. 1 Feb 1972*.

[27] J .N. Price & D. Hull, "Effect of Matrix Toughness on Crack Propagation during Stress Corrosion of Glass Reinforced Composites," *Composites Science & Technology 28(1987) 193-210.*

[28] Hogg, P.J. & Hull, D., "Micromechanism of Crack Growth in Composite Materials under Corrosive Environments," *Metal Sc.,* Aug-Sept. 1980, pp 441-449.

[29] G. Lewis, S. W. Bedder & I. Reid, "Stress Corrosion of Glass Fibers in Acid Environments," *Journal of Materials science Letters* 3(1984) 728-732.

[30] R.F. Regester, *Corrosion-NACE*, vol. 25, no. 4, April, 1969, p. 157.

[31] L.S. Norwood, Polyester Resins in Corrosive Environments, *Pipe Conference, 1980.*

[32] H. Thomas, Jonathan Bartley-Cho, Seung Gyu Lim, “The Effect of Loading Parameters on Fatigue of Composite Laminates: Part II” *Final Report U.S. Dept. of Transportation July, 1997.*

[33] Lutz Hohne & Christine Ullner, Modelling of Time Strength Behaviour of Soda-lime-silica Glass in Moist Environments, *Glass Technology 67 (1994) No. 8*

[34] J.F. Mandell & U. Meier, Effects of Stress Ratio, Frequency, Loading Time on Tensile Fatigue of Glass-Reinforced Epoxy, *Long-Term Behavior of Composites, ASTM STP 813, T. K. O’Brien, ed. American Society for Testing and Materials, Philadelphia, 1983, pp. 55-77.*

[35] A. Rotem, “Load Frequency Effect on the Fatigue Strength Isotropic Laminates,” *Composites Science and Technology*, 46, 1993, pp. 1129-138.

[36] K. Jakus, J.E. Ritter, Jr., & J.M. Sullivan, *J. Am. Ceram*. Soc., 64, 372, 1981. Ed. Charles R. Kurkjian, Plenum Press.

[37] G. D. Sims & D. G. Gladman, “Effect of Test Conditions on the Fatigue Strength of a Glass-Fabric Laminate: Part A-Frequency,” *Plast. Rubb. Mater. Appl. 1, 41-48 1978*

[38] G. D. Sims &D. G. Gladman, “Effect of Test Conditions on the Fatigue Strength of a Glass-Fabric Laminate: Part B-Specimen Condition,” *Plast. Rubb. Mater. Appl. 1, 122-128 1980.*

[39] C. J. Jones, R. F. Dickenson, et al., The Environmental Fatigue Behavior of

Reinforced Plastics, *Proc. R. Soc. Lond. A 396, 313-338* (1984).

[40] C. Demers, E-glass Fiber-Reinforcement Polymeric Composites, Tension-Tension Axial Fatigue Life Diagram, *The National Seminar on Advanced Composite Material Bridges May 5-7, 1997, FHWA Sponsor*.

[41] Fred McBagonluri, M. Hayes, K. Garcia & J.J. Lesko, “Fatigue Behavior of High Performance Polymeric Composites in a Simulated Seawater Environment”, *Progress Report to National Institute for Standards and Technology*, Gaithersburg, MD.Dec.1997.

[42] Fred McBagonluri & J.J. Lesko, “The Effect of Frequency of Fatigue Cycling & Applied Stress Level on Temperature Change in a Glass/Vinyl Ester Composite Coupon”, *Progress Report to the National Institute for Standards and Technology*, Gaithersburg, MD. May 1997.

[43] R. E. Mould & R. D. Southwick, *J. Am. Ceram. Soc.*, 42, 532, 1959.

[44] J.E. Ritter,, Jr. & C. L. Sherburne, *J. Am. Ceram. Soc.*, 54, 601, 1971.

[45] J.E. Ritter,, Jr. & J. Manthurithil, *Glass Technology*, 14, 60, 1973.

[46] R.H. Doremus, *Glass Science*, J. Wiley & Sons, N.Y., 1974.

[47] B. A. Proctor, I. Whitney & J.W. Johnson, *Proc. Roy. Soc*. A, 297, 534, 1967.

[48] D.L. Hollinger, W.G. Kanetzky & H.T. Plant. *Report AD 607040,* pp. 12, 1964.

[49] D. Kalish & B.K. Tariyal, *J. Am. Ceram. Soc*., 6, 518, 1978.

[50] S. Sakaguchi & T. Kimura, *J. Am. Ceram. Soc.*, 64, 259, 1981.

[51] H.C. Chandan & D. Kalish, *J. Am. Ceram. Soc.*, 65, 171, 1982.

[52] S. W. Wiederhorn et al. "An Error Analysis of Failure Prediction Techniques Derived from Fracture Mechanics," *J. Am. Ceram. Soc.* 59, 403-411 (1976).

[53] L. N. McCarthey, Time-dependent Strength of Large Bundles of Fibers Loaded in Corrosive Environment, *Fiber Science & Technology, Applied Science* Publishers, England: 1982.

[54] L.J. Broutman & S. Sahu, "A new theory to predict cumulative fatigue damage in fiberglass reinforced plastics," *Composite Materials: Testing and Design (Second Conference), ASTM STP* 497:170 (1970).

[55] Fred McBagonluri, Mike Hayes, K. Garcia, J. J. Lesko, "Durability of E-glass Vinyl Ester an Elevated Temperature Simulated Sea Water Environment," *Proceedings of the*

Seventh International Conference on Marine Applications of Composite Materials (MACM '98) Melbourne, Fl March 17-19, 1998.

[56] Fred McBagonluri, Mike Hayes, K. Garcia, J. J. Lesko, *Durability of Glass/Vinyl Ester Composites in a Simulated Sea Environment*, Proceedings of the American Society of Mechanical Engineers (ASME) Conference Dallas, TX 15-18 Nov. 1997.

[57] J. J. Lesko, Mike Hayes, Fred McBagonluri, K. Garcia, *Environmental-Mechanical Durability of Glass/Vinyl Ester Composites in Progress in Durability Analysis of Composite Systems,* Proceedings of the International Conference on Durability of Composites Systems (DURACOSYS) Blacksburg, VA 1997.

[58] Glenn G. Foster, "Tensile & Flexure Strength of Unidirectional Fiber-Reinforced Composites: Direct Numerical Simulations and Analytic Models," *MS Thesis Virginia Tech* February 1998.

[59] [9] B. A. Proctor, I. Whitney, and J. W. Johnson, "Strength of Fused Silica," *Proc. Roy. Soc.* (London) A297, 534-557 (1967).

[60] Robert Jones, Mechanics of Composite Materials, 1975.

[61] David Hartman et al., "High Strength Glass Fibers," Technical Paper Owens Corning Pub. No. 1-PL-19025-A July 1996.

[62] R. Brückner, “Properties & Structure of Vitreous Silica,” I. J. Non-Cryst Solids 5: 123-75. 1970.

[63] R. Brückner, “Properties & Structure of Vitreous Silica,” I. J. Non-Cryst Solids 5: 177-216. 1971.

[64] F McBagonluri, G. Foster, S. Case, J. Lesko, B. Curtin, “Micromechanics Based Life Prediction of Glass-Reinforced Composites,” *Proceedings of the International Conference for the Society for Experimental Mechanics*, Houston, TX, June 3 1998.

[65] Handbook of Fiberglass & Advanced Plastics Composites, Ed. George Lubin, Krieger, Huntington: NY, 1969.

[66] Life Prediction Methodologies for Composite Materials, National Materials Advisory Board Commission on Engineering & Technical Systems National Research Council, 1991.

[67] X. Dirand et al., Interfacial Shear Strength in Glass-Fiber/Vinyl Ester-Resin Composites,” Composites science & Technology 56 (1996) 533-539.

Chapter 8 : VITA

The author, David Fred McBagonluri-Nuuri, was born on August 18, 1970, in Accra, Ghana to David Ang-Laara MacBagonluri and Patience A. Nuuri. Fred is the grandson of Chief Ollo Naa Bagonluri I (1951-1974) of the Ollo Traditional Area in the Upper-West Region of Ghana, and Queen Nayirima. He graduated from the St. Louis Preparatory School in 1985. In 1990, he obtained the General Certificate of Education and School Certificate (GCE/SC) from Nandom Secondary School with a *Division I Distinction,* and proceeded to the prestigious St. Augustine's College in Cape Coast, Ghana, where he did is pre-medical studies in Functional Biology, Physics and Chemistry. From 1991 to 1996 Fred was Ghana Government Presidential Scholar at Central State University in Ohio, from where he graduated *summa cum laude* with a BSMFE in Manufacturing Engineering. Upon completing his Masters in Engineering Mechanics in August, he proceeds to the University of Dayton, Ohio to pursue the Ph.D. in Materials Engineering. The author's interests include fatigue and creep simulation, modeling of glass-reinforced composites for application in infrastructure and offshore platforms, solid modeling, mechanical design and experimental mechanics.